FRONT MATTER

Point-of-care applicable metabotyping using biofluid-specific electrospun MetaSAMP®s directly amenable to ambient LA-REIMS

Direct biofluid metabotyping using MetaSAMP®

Authors

Margot De Spiegeleer[1], Vera Plekhova[1], Jozefien Geltmeyer[2], Ella Schoolaert[2], Beata Pomian[1], Varoon Singh[1], Kathleen Wijnant[1], Kimberly De Windt[1], Volter Paukku[1], Alexander De Loof[3], Inge Gies[4], Nathalie Michels[5], Stefaan De Henauw[3], Marilyn De Graeve[1], Karen De Clerck[2], Lynn Vanhaecke[1,6,†,*]

Affiliations

[1]Laboratory of Integrative Metabolomics, Department of Translational Physiology, Infectiology and Public Health, Ghent University, Belgium.

[2]Department of Materials, Textiles and Chemical Engineering, Faculty of Engineering and Architecture, Ghent University, Belgium.

[3]Department of Public Health and Primary Care, Faculty of Medicine and Health Sciences, Ghent University, Belgium.

[4]Department of Pediatrics, Vrije Universiteit Brussel (VUB), Universitair Ziekenhuis Brussel (UZ Brussel), Belgium.

[5]Department of Developmental, Personality and Social Psychology, Ghent University, Belgium.

[6]Institute for Global Food Security, School of Biological Sciences, Queen's University, United Kingdom.

***Corresponding author**

Prof. Dr. Lynn Vanhaecke

ORCID 0000-0003-0400-2188

Laboratory of Integrative Metabolomics

Department of Translational Physiology, Infectiology, and Public Health

Faculty of Veterinary Medicine, Ghent University,

Salisburylaan 133, B-9820 Merelbeke, Belgium

Tel: +32 9 264 74 57

E-mail: Lynn.Vanhaecke@UGent.be

Abstract

In recent years, ambient ionization mass spectrometry (AIMS) including laser ablation rapid evaporation IMS (LA-REIMS), has enabled direct biofluid metabolome analysis. AIMS procedures are however still hampered by both analytical, *i.e.*, matrix effects, and practical, *i.e.*, sample transport stability, drawbacks that impede metabolome coverage. In this study, we aimed at developing biofluid-specific metabolome sampling membranes (MetaSAMP®s) that offer a directly applicable and stabilizing substrate for AIMS. Customized rectal, salivary and urinary MetaSAMP®s consisting of electrospun nanofibrous membranes of blended hydrophilic (polyvinylpyrrolidone and polyacrylonitrile) and lipophilic (polystyrene) polymers supported metabolite ab-, ad-, and desorption. Moreover, MetaSAMP® demonstrated superior metabolome coverage and transport stability compared to crude biofluid analysis and was successfully validated in two pediatric cohorts (MetaBEAse, N=234 and OPERA, N=101). By integrating anthropometric and (patho)physiological with MetaSAMP®-AIMS metabolome data, we obtained significant weight-driven predictions and clinical correlations. In conclusion, MetaSAMP® holds great clinical application potential for on-the-spot metabolic health stratification.

Teaser

Customized biofluid-specific MetaSAMP®s enable superior metabolome coverage and stability for direct health stratification.

MAIN TEXT

Introduction

To date, metabolomics of human biofluids is emerging as a promising biofocus as it provides advantages that classical diagnostics do not, following discovery of a suite of clinically relevant biomarkers that are simultaneously affected by disease while contributing to the elucidation of metabolic pathways underlying particular phenotypes of health and disease (*i.e.*, metabotyping) (*1–3*). The most urgent application of metabolomics remains the identification of pathologies in children as early-infancy exposures, including nutrition and illness severely impact adult health and functionality as well (*4*). In this respect, metabolite patterns offer a valid tool to profile individuals (*5*) at risk of developing *e.g.*, the metabolic sequelae coinciding the global rise in overweight and obesity (*6*) by discerning between metabolically healthy and unhealthy

phenotypes and predict future risks of developing co-morbidities such as (pre)diabetes, metabolic syndrome, etc. (*2*, *7–10*).

The urinary and fecal metabolomes have been popularized as they reflect both exogenous and endogenous metabolic products (*11*), as well as complex interactions between dietary intake, gut microbiome and host (*12*). Salivary metabolites largely mirror those in blood and may thus reflect many pathophysiological and nutritional changes, as well as exposure to medication and environmental factors (*13*). Major bottlenecks in large metabolomics cohort studies remain the collection, transport, storage and sample preparation of biofluids. Indeed, ongoing (bio)chemical reactions following sample collection, long-term preservation and extraction may substantially introduce metabolome alteration (*12*, *14*) and misleading interpretations, while the addition of chemical preservatives during shipping, storage and extraction causes metabolome contamination by adduct formation and/or ion pairing (*15*).

The typical workflow used in conventional biofluid metabolomics comprises multiple time-consuming steps including sample collection and pretreatment such as lyophilization, extraction and chromatographic separation, etc., resulting in low sample throughput (ca. 60/day) and high costs (> 200 euro/analysis) (*16*). During the last decades, instrumental advances have allowed the integration of near-real-time surface sampling or ambient ionization (AI) of matrices in their native analyte environment (*17–19*). Laser ablation coupled to rapid evaporative ionization mass spectrometry (REIMS), termed laser-assisted REIMS (LA-REIMS), is among the few ambient ionization-based techniques that have found their way into the clinic both *in vivo* and *ex vivo* (*16*, *20*). LA-REIMS uses a sample-focused laser beam that excites the most intense vibrational band (oxygen-hydrogen stretching mode) of water molecules present in the sample, initiating ablation heat and causing evaporation. The resulting analyte-containing aerosol is aspirated towards the MS under the instrument's vacuum where it is mixed with a solvent and collides with a heated collision surface to form gas-phase ions for analysis (*16*, *20*). To date, LA-REIMS is the only AIMS platform that has been successfully employed for the automated analysis of a range of crude biofluids, including feces, saliva, urine, etc. (*1*). Indeed, LA-REIMS enables an analysis rate of only few min per sample, and demonstrates substantial congruencies with mass spectra obtained by conventional metabolomics (*16*, *21*, *22*). Current challenges in direct LA-REIMS-based crude biofluid analysis are the existence of matrix effects and reduced ionization efficiency, resulting in a decreased selectivity and thus metabolome coverage (*23*). Moreover, biofluid collection may hamper a direct sampling-to-MS result workflow (*1*), because the need to wait for *e.g.*, defecation prevents immediate sample availability. A sampling device that allows the integration of sampling, sample

preparation and presenting the sample for direct metabolomics analysis, would offer a substantial advance compared to crude biofluid analysis, because it would largely circumvent these challenges.

In this study, we aimed at developing, optimizing and benchmarking biofluid-specific samplers (MetaSAMP®s, WO2021/191467) for direct rapid AIMS-based metabotyping (Fig. 1A). Our MetaSAMP®s consist of nanofibrous membranes customized both in terms of polymer composition, ratio and fiber diameter by electrospinning (ES) towards optimal biofluid-specific (feces, saliva and urine) metabolome sampling, ab- and adsorption, and stabilization. ES is a simple and versatile technology that uses electrostatic forces to produce (nano)fibrous membranes with controllable compositions (*24*, *25*). The typical porous bed structure of electrospun membranes enables analyte enrichment due to highly efficient mass transfer between biofluids and the polymerous (nano)fibers, which act as sorbents, facilitating metabolite microextraction (*26*, *27*). The possibility of including specific chemical moieties offers a means to enhance the ab- and adsorption of analytes bearing a broad range of polarities (*28*). Moreover, biocompatible polymers such as polyacrylonitrile (PAN) are also suitable for ES, which allows for *in vivo* usage while supporting the exclusion of macromolecules (*29*). The MetaSAMP®s may be configured as a sampling kit with an integrated electrospun membrane whether or not assisted by a medical swab that is directly amenable to our established rapid LA-REIMS platform (*1*) (Fig. 1A). We also confirmed the ability of MetaSAMP®s to stabilize the biofluid-specific metabolome, increasing transport ease and duration. Finally, the clinical applicability and superior performance of our MetaSAMP®s relative to the analysis of crude biofluids, were assessed *ex vivo* in 2 pediatric cohorts (MetaBEAse and OPERA). As such, we have demonstrated that direct MetaSAMP®-based biofluid metabotyping may have far-reaching potential as a future medical device.

Results

Optimized electrospun membranes for biofluid-specific metabolic fingerprinting: MetaSAMP®s

The development of our biofluid-specific metabolome sampling MetaSAMP®s started by tuning the configuration and chemical composition of the core biofluid-specific membrane (feces, saliva and urine, Fig. 1B) towards maximal metabolome coverage following LA-REIMS analysis (wide logP span and molecular feature count) and repeatability (as % of molecular features with a CV≤30%). Hereto, the electrospun core membranes were fabricated using a rotating drum collector (Fig. 1C) on an aluminium support layer (Fig. 1B). Because the superiority of materials with a hydrophilic-lipophilic balance (HLB) as comprehensive metabolome ab- and adsorptive sorbents

has been reported (*28*, *30*), we selected two relevant HLB polymers (PVP and PS) for our core membranes. As feces (and rectal content) are more heterogenous, complex and richer biofluids than saliva (*13*) or urine (*11*), the rectal MetaSAMP® optimization was prioritized. Following impregnation with porcine rectal content, different core membrane polymer compositions were evaluated for their metabolome coverage using LA-REIMS analysis as detailed in note S1.1 and inspected through scanning electron microscopy (SEM) analysis (fig. S1). The usage of porcine rectal content was rationalized based on similarities in nutrition and metabolism between pigs and humans (*31*). It was observed that a balanced blend of PVP/PS (50/50, *w/w*) significantly outperformed (ANOVA FDR-adjusted p=9.03e^{-8}, F=41.44, df=5) the other compositions tested in terms of metabolome coverage while providing acceptable repeatability (note S1.1 and fig. S2). Consequently, the HLB of the core membrane's compositional fibers was demonstrated through modulated differential scanning calorimetry (mDSC). Separate glass transition temperatures (Tg) could be assigned to carbonyl- (PVP) and benzene-rich (PS) moieties (*32*) (note S2 and fig. S3). Additionally, the LA-REIMS settings were further optimized for rectal MetaSAMP® analysis using a design of experiments (DOE) approach (note S3.1). Significance (ANOVA FDR-adjusted p=0.012 and p<0.001, F=14.62 and 25.35, df=5) was detected for higher scan time and solvent flow rate. The optimal values were obtained by maximizing metabolome coverage, molecular feature signal intensity and repeatability, resulting in a scan time of 0.7 scans s^{-1} and a solvent flow rate of 250 µL min^{-1} (table S1 and fig. S4).

Hereafter, electrospun PVP/PS membranes were tested for saliva and urine (note S1.2). When spiking the PVP/PS core membranes comprising 50-100% PS with saliva or urine, unacceptable long biofluid residence times were noted (> 1h). This could be ascribed to the more aqueous nature of the biofluids saliva and urine as compared to the pig rectal content tested earlier. Interestingly, more homogenous nanofiber size distributions were observed for the different core membranes' composition with increasing hydrophilic PVP (10% or more) (fig. S5), which would benefit the reproducibility of LA-REIMS metabolomics analysis. Because these increased biofluid residence times were observed to bring about more variable impregnation times and thus unacceptable variation in obtained LA-REIMS metabolic fingerprints and because of the size distribution data (fig. S5), we decided to additionally evaluate the inclusion of the highly polar PAN polymer as a cover layer for our MetaSAMP® and later in the core membrane blends for saliva and urine, as this polymer may increase the wettability (*33*) and thus speed of analysis upon inclusion (see below). Instrumental settings for LA-REIMS analysis of impregnated electrospun membranes with saliva and urine were the same as in our previously biofluid-specific optimized protocol (*1*) (table S1).

Next, we investigated the potential of a PAN cover layer considering the future rectal MetaSAMP®'s *in vivo* usage in a sampling kit or medical swab. Indeed, on top of its high polarity and thus wetting capabilities for aqueous matrices (*33*), PAN is also a biocompatible polymer with documented *in vivo* applications (*34*, *35*) that has previously been demonstrated to facilitate selective transport of small molecules to ab- and adsorptive polymers by partially diminishing surface (bio)fouling mechanisms for molecules >1.5 kDa and completely preventing access to molecules >7 kDa (*29*, *36*). As a result, a PAN cover layer was hypothesized to enhance core membrane stability as surface functionalities of the PVP/PS microporous core are expected to be less susceptible to oxygen or moisture in its presence. For this experiment, pooled quality control (QC) fecal samples were used, enabling the evaluation of our future target matrix and thus reproducibility of the entire analysis protocol best. Indeed, feces shows substantial similarity with rectal content with respect to bacterial community structure and functionality (*37*, *38*). Hereto, PAN was tested at various concentrations (5-15%, *w/w*) and evaluated for its solution viscosity, quality of the PAN electrospun fiber network and fiber size distribution (table S2). Optimal small molecule sampling and subsequent analysis were strived at by retaining the average fiber diameter and its distribution as low as possible in effectively excluding macromolecules like proteins and DNA. The combination of an acceptable average fiber diameter of 384 nm and a smooth fiber network without bead formation as observed by SEM (fig. S6-S8 and table S2), rationalized our choice to use 10% (*w/w*) PAN in further experiments.

To confirm the optimal position of the electrospun PAN layer, the effect of varying its position relative to the core membrane (PVP/PS) was tested. The effects of an electrospun PAN cover layer added to the PVP/PS electrospun core membrane both with and without including PAN as a bottom layer on the aluminium support were examined in terms of metabolic coverage (ranging from 50-1200 Da) and repeatability. To identify which metabolite classes were impacted by the presence of PAN cover and bottom layers, the measurable mass range was subdivided into six subsets, including a subset covering 50-200 Da, encompassing low-molecular-weight metabolites such as carbohydrates and short-chain fatty acids; two subsets covering 200-600 Da, encompassing medium-, long- and very-long-chain fatty acids as well as amino acids, diacylglycerols, and sphingolipids; two subsets covering 600-1000 Da, encompassing phospholipids a.o. (*16*, *18*, *39*), and a subset covering 1000-1200 Da, mainly encompassing saccharolipids and glycosphingolipids (*40*). Indeed, from a metabolic health perspective (*2*), metabolite classes covering all those mass ranges are relevant. The impregnated electrospun core rectal MetaSAMP® layer covered by an additional electrospun PAN layer gave significantly (p<0.001) higher metabolome coverage, ion intensities and molecular feature count following LA-REIMS analysis compared to the analysis of

the crude biofluid (fig. S9 and table S3). It was also observed that the PAN cover layer enhanced the spreading and therefore penetration of fecal water (fig. S10) as confirmed by smaller CAMs (50±2° *vs.* 144±4°) (fig. S11 and table S4). As a result, the increased hydrophilicity/wettability brought about by the electrospun PAN cover layer could promote beneficial chemical and physical interactions and hence efficient mass transfer between biofluid metabolites and the core membrane (fig. S12), as seen before in (micro)porous applications with high surface area (*26*, *27*, *41*).

Because the core membrane's ab- and adsorptive capabilities were expected to be affected by the PAN cover layer, a second optimization round was initiated for obtaining the final composition of each biofluid-specific MetaSAMP® using a D-optimal experimental design (table S5). To this end, average fiber diameter and morphology, metabolome coverage, and repeatability were evaluated as endpoints. The core membrane composed of PVP/PS (60/40, *w/w*) with 8% (*w/w*) polymer weight% covered by PAN showed the highest metabolome coverage and repeatability upon LA-REIMS for fecal water (table S5 and fig. S13A-C). For saliva, the PVP/PS (20/80, *w/w)* membranes showed the highest metabolome coverage and repeatability with the most stable fibers at 12% (*w/w*) polymer weight%, while for urine, the different membranes behaved similarly with a tendency towards better repeatability for the PVP/PS (20/80, *w/w)* as well (table S5). Because 20% PVP was the lowest tested, an additional experiment was performed for urine and saliva with 0-20% PVP while including 0-10% PAN in the blend (table S6). The core layers comprising PVP/PS (10/90) and PVP/PS/PAN (20/70/10) both with 12% (*w/w*) total polymer weight% covered with a PAN layer, were finally selected because higher salivary and similar urinary metabolome coverage and repeatability (95% and 97% of features with CV≤30% for saliva and urine, respectively) (fig. S13D-I) were achieved compared to crude analysis of saliva and urine, while no damage to the electrospun fibrous core blends was observed, suggesting morphological integrity even after prolonged biofluid exposure (>15 min) (fig. S14). Our three final optimized rectal, salivary and urinary MetaSAMP®s comprised of, respectively, blends of electrospun PVP/PS 60/40, PVP/PS 10/90, and PVP/PS/PAN 20/70/10 covered with an electrospun PAN layer. In addition, the evaluation of different impregnation volumes (20-100 µL) and times pointed toward 30 µL or its equivalent in droplets (3) and 10-15 min as the optimal parameters (note S1.3 and fig. S15).

Direct MetaSAMP®-LA-REIMS offers a richer metabolic fingerprint than crude biofluid LA-REIMS

Following optimization, we aimed at demonstrating the advantages of direct MetaSAMP®-LA-REIMS metabolic fingerprinting compared to crude biofluid LA-REIMS analysis in terms of metabolome coverage using impregnated rectal, salivary and urinary MetaSAMP®s from

participant children covering all IOTF scores (pooled QC samples, *N*=3, MetaBEAse cohort for the rectal and urinary MetaSAMP® and OPERA cohort (*42*) for the salivary MetaSAMP®) (Table 1). Richer mass spectra were observed in impregnated MetaSAMP®s compared to the crude biofluid LA-REIMS metabolic fingerprints (Fig. 2A-C). The numbers of metabolic features counted (20 technical replicates), respectively, for the rectal, salivary and urinary MetaSAMP®s and feces, saliva and urine were 2078±11.05, 2150±4.10 and 1697±3.95 and 1896±2.57, 1960±3.12 and 1477±8.31 (data S1-S3, significantly different, independent samples *t*-test p=0.02, 5.60 e^{-6} and 2.08 e^{-4}). Also, higher overall signal intensities (TIC) were measured for the respective MetaSAMP®s (data S4-S6). Additionally, since metabolite classes covering the aforementioned mass ranges are clinically relevant with regard to the metabolic disturbances underlying overweight and obesity (*2*), metabolome coverage was also evaluated throughout the different mass ranges in further evincing higher overall signal intensities. As such, palmitic acid (fatty acid, *m/z* value of 255.2 Da, logP 6.4), 1-heptadecanoyl-2-(9Z,12Z,15Z-octadecatrienoyl)-sn-glycerol (glycerolipid, *m/z* value of 603.5 Da, logP 13.4) (Fig. 2A) and a putatively identified lipid (ceramide sphingolipid or phosphoethanolamine glycerophospholipid, *m/z* value of 736.5 Da) (Fig. 2B), were detected by our MetaSAMP®-LA-REIMS. As demonstrated via radar charts for each of the mass ranges, higher coverage was noted upon analysis with the biofluid-specific MetaSAMP®s as compared to the crude biofluids (Fig. 2A-C) for most mass ranges. No ions could be detected that were caused by the interaction between the laser ablation process and the membrane polymers at the optimized biofluid-specific MetaSAMP®-LA-REIMS analysis conditions (note S4 and fig. S16-S17).

In conclusion, our optimized biofluid-specific MetaSAMP®s confirmed superior metabolome coverage across a broad mass range (50-1200 Da) and wide logP span compared to the analysis of crude biofluids.

Biofluid-specific MetaSAMP®s improve short-term metabolome stability and speed

Biofluid collection and transport, especially in large cohorts, is not straightforward. In the case of fecal samples, the need to wait for defecation prevents the direct analysis, inferring the need of biobanking (and thus freezing). The addition of chemical preservatives to crude biofluids for shipping and storage stability negatively impacts the metabolome's accuracy (*12*, *14*). Our optimized rectal, salivary and urinary MetaSAMP®s were hypothesized to conserve a more accurate snapshot of the metabolome during storage and are directly amenable to sample preparation-free metabolomics analysis, as such lowering the individual time and cost per analysis. The storage period was set at 48 h, which corresponds to the maximum transport duration from the patient's home or physician's office to the laboratory in Western countries (*e.g.*, with courier services). To

address this, metabolome coverage and repeatability based on crude biofluid fingerprinting (pooled QC samples, *N*=6) and their corresponding impregnated MetaSAMP®s were measured at room temperature (RT), i.e., 22±2°C and 4°C and the total sampling and analysis times were recorded. Closer correlations in the LA-REIMS results were observed between 48 h stored samples and those analyzed immediately after collection using the optimized MetaSAMP®s stored at 4°C when compared to the corresponding correlations of the data obtained with their crude counterparts (Fig. 3A). At RT, however, both crude biofluids and MetaSAMP®s brought about substantial metabolome changes as confirmed by low repeatability values (<50% of features with CV ≤30%). Subsequently, intraclass correlation coefficients (ICC) intervals were computed to investigate metabolome variation between time points, considering molecular features with ICC values ≤0.4 as more unstable over time (*43*). Upon storage at 4°C, 1371 (feces) *vs.* 1850 (rectal MetaSAMP®), 2460 (saliva) *vs.* 3397 (salivary MetaSAMP®), and 2677 (urine) *vs.* 2721 (urinary MetaSAMP®) molecular features remained stable (ICC >0.4) (Fig. 3B). Moreover, the total analysis time of the optimized biofluid-specific MetaSAMP®-LA-REIMS methodology was recorded as <20 min per sample (<15 min for sampling incl. impregnation and 5 min for the LA-REIMS analysis workflow) compared to <40 min per sample for the LA-REIMS analysis of crude biofluids, aside from the transport time for both methodologies (and lyophilization of feces for the LA-REIMS analysis of crude feces) (*1*, *12*, *16*). In conclusion, our MetaSAMP®s generally demonstrated a superior number of stable molecular features over time and provide an efficient means for rapid LA-REIMS-based metabotyping.

Direct biofluid-specific MetaSAMP®-LA-REIMS is a clinically valid metabotyping tool

Metabolomics analysis has substantial value in a plethora of metabolic and food-related diseases (*2*, *44*). Metabolite patterns could therefore offer a valid tool to profile individuals at high risk of developing *e.g.,* obesity-related metabolic diseases, *i.e.,* discerning between metabolically healthy and unhealthy phenotypes already at young age (*2*, *5*). To provide proof-of-principle for the clinical potential of our MetaSAMP®-LA-REIMS in childhood overweight and obesity, MetaSAMP®-derived metabolic fingerprints of biofluids obtained in two pediatric cohorts: MetaBEAse (feces and urine of children aged 6-12 years) and OPERA (*42*) (saliva of children aged 6-16 years), were investigated in terms of discrimination and predictive potential. For this purpose, a large set of anthropometric and clinical measurements were performed (Table 1) to link potentially relevant metabolite discrepancies in overweight and obese children and pathophysiological processes.

First, the discriminative and predictive performance of LA-REIMS analysis was compared between crude biofluids and their impregnated MetaSAMP®s. By doing so, more subtle effects related to subclinical pathology, *i.e.*, metabolic perturbations due to increased weight and/or adiposity, were visualized by valid orthogonal projection to latent structures discriminant analysis (OPLS-DA) models using the international obesity BMI cut-off for thinness, overweight and obesity (IOTF) as a classifier (Fig. 4A-C). Interestingly, a similar or even greater number of molecular features that were significantly differentiated based on their value of variable importance in projection (VIP) for the OPLS-DA models constructed (table S7) were retrieved for the analysis of the MetaSAMP®s as compared to that of the crude biofluids. The same was noted for the validation parameters (CV-ANOVA $p< 0.05$, good permutation testing (N=100), goodness-of-fit and predictive performance of the model reflected by R^2(cum)>0.8 and Q^2(cum)>0.4 for biological data), respectively (table S7). These findings provide evidence that discriminative categorization based on metabolic fingerprints was mostly superior using the biofluid-specific MetaSAMP®-LA-REIMS methodology. Furthermore, its predictive potential for overweight classification using IOTF scores was assessed by logistic regression. This approach was only applied to the MetaBEAse cohort data because the sample size of the OPERA cohort (N=101) did not sustain good model building (*45*). Metabolic fingerprints detected by rectal (Fig. 4D) and urinary (Fig. 4E) MetaSAMP®-LA-REIMS analyses enabled predictive IOTF classification. We observed strong predictive potential (area under the curve (AUC) range 0.84-0.96) when all overweight (including obese) children as well as only obese children were included and compared to a balanced number of normal weight children, suggesting the early onset, *i.e.*, already in overweight (not yet obese) children, of metabolic divergences (*2*).

To further clinically validate our MetaSAMP®-LA-REIMS metabotyping approach, Spearman correlations were calculated between normalized levels of molecular features captured with each biofluid-specific MetaSAMP® and anthropometric and clinical measurements from both cohorts (MetaBEAse and OPERA). Interestingly, among anthropometrics, adiposity measures (BMI-*z*, IOTF, waist circumference (Waist) and waist-to-height ratio (WHR)) that are related closely to overweight metabotypes (*46*) showed the highest Spearman ρ-values with fecal, salivary and urinary metabolic profiles in both cohorts (Fig. 4F-H). A number of clinically relevant end points, *e.g*, lipid, glycemic, inflammatory and hormonal blood markers, showed moderate to good correlations (Spearman ρ-values 0.4-0.6) (*47*) with biofluid-specific MetaSAMP®-derived metabolic fingerprints. For instance, glucose and insulin (-like growth factor 1) in blood, which have been associated with insulin resistance (*48*), and SHBG and DHEAS, which have been negatively associated with adiposity and low-grade inflammation in childhood obesity (*49*, *50*),

correlated well with rectal and urinary MetaSAMP®-derived fingerprints (Spearman ρ-values up to 0.5, Fig. 4F-H) (MetaBEAse cohort). Adipokine hormones with appetite suppressing and initiating effects, such as leptin and ghrelin, respectively (*51*), revealed moderate to good correlations (Spearman ρ-values up to 0.4, Fig. 4G) with metabolic fingerprints obtained by our salivary MetaSAMP® (OPERA cohort), and hence were influenced by adiposity and insulin sensitivity (*52*). Collectively, these results suggest that our MetaSAMP®s allow capturing multiple clinically relevant metabolites of energy, immune and lipid metabolism.

As a final step in demonstrating the clinical potential of our MetaSAMP®-LA-REIMS, the identification of molecular features that showed significant (p<0.05, Wilcoxon rank-sum test with continuity correction) Spearman correlations with anthropometric and/or clinical parameters based on MetaSAMP®-LA-REIMS analysis was pursued. We focused on the rectal MetaSAMP® data (MetaBEAse cohort) because feces comprises the most complex matrix and is considered most relevant to capture gut-microbiome-diet interactions (*12*). This is, the role of the microbiome and its metabolites in obesity have been ubiquitously reported in literature (*2*, *53–55*). Hierarchical Ward-linkage clustering analysis was used to unveil unique molecular features clustering according to their shared correlation structure (Fig. 5A, Wilcoxon rank-sum test with continuity correction to assess which correlations were significant with p<0.05). Annotation of potentially clinically relevant molecular features originating from the rectal MetaSAMP®-LA-REIMS fingerprints (data S7), resulted in the identification of acylcarnitines, fatty acids, an amino acid and a cholesterol derivate, *i.e.*, 7-ketocholesterol, 12-tridecenoic acid, (iso)valeryl-L-carnitine, L-carnosine, myristoleic acid, N-acetylglutamic acid, O-succinyl-L-carnitine, and sphingosine. Subsequently, we assessed if those metabolites significantly (p<0.05, Kruskal-Wallis test with Dunn's post-hoc test) changed between different weight groups. Out of the 81 molecular features determined with rectal MetaSAMP®-LA-REIMS in negative ion mode (Fig. 5A), 8 metabolites were found to correlate with and contribute to the discrimination of weight classification in children of which 6 were significantly different between normal weight, overweight and obese children (Fig. 5B). Furthermore, the 8 annotated metabolites could be detected by LA-REIMS analysis of both crude feces and rectal MetaSAMP®, yet their normalized intensity values were generally higher when using the rectal MetaSAMP® compared to crude fecal analysis (Welch two-sample *t*-test or Wilcoxon rank-sum test, p<0.05) and the metabolites were thus more reliably detected (fig. S18).

Physicochemically diverse clinically relevant metabolites can be reproducibly detected using rectal MetaSAMP®-LA-REIMS

Finally, in assessing the future clinical implementation of MetaSAMP®s, a targeted approach was implemented using the rectal MetaSAMP® on a selection of clinically relevant metabolites in (childhood) overweight and obesity (*2*) according to FDA recommendations (*56*). The latter was performed with analytical standards that were selected based on their plausible natural occurrence in feces (*57*) covering a broad polarity and mass range (100-1200 Da and logP of -4 to 13, table S8). The targeted detectability, technical precision, repeatability and intermediate precision of these analytes were determined by applying 3 consecutive ablation events per membrane piece (N=5) on two different days and calculating the number of molecular features upon LA-REIMS analysis (table S9 and data S8). Additionally, the standards were spiked directly onto the rectal MetaSAMP® (table S9) and, hereafter, onto the impregnated rectal MetaSAMP®s (table S10) using a pooled sample (from MetaBEAse, N=3). Regarding the latter, intra- and interassay CVs were below the threshold (<30%) for respectively 9 and 7 (table S10) out of the 11 metabolites that were initially detected when spiked into solvent. In conclusion, our results showcase that a diverse range of clinically relevant metabolites may be sufficiently reproducibly detected using rectal MetaSAMP®-LA-REIMS.

Discussion

In this work, customized biofluid-specific metabolome samplers, called MetaSAMP®s, were developed for direct user-friendly sampling, ab- and adsorption and stabilization of complex human biofluids including feces, saliva and urine. The hyphenation of these optimized MetaSAMP®s with our automated LA-REIMS platform (*1*) enables direct sampling and analysis of the respective metabolomes in less than 20 min per sample (Fig. 1A) and provides a richer and more stable reflection of the biofluid-specific metabolome as compared to crude biofluid analysis. Indeed, the MetaSAMP®-LA-REIMS metabotyping approach represents a superior alternative to crude biofluid LA-REIMS analysis regarding on-the-spot metabolic health stratification and holds great potential for usage in large cohort metabolomics studies. We have therefore successfully evaluated its clinical implementation in the context of the childhood obesity pandemic (*6*) using fecal, salivary and urinary metabotyping in samples obtained from two pediatric cohorts (MetaBEAse and OPERA). Although our MetaSAMP®-LA-REIMS methodology centers on untargeted metabolic fingerprinting using HRMS, we also demonstrated reproducible targeted analysis of a selection of physicochemically diverse metabolic disease-related metabolites.

The respective biofluid-specific rectal, salivary and urinary MetaSAMP®s comprised a core layer that was optimized towards maximal metabolome coverage as a blend of HLB electrospun nanofibrous polymers, *i.e.*, PVP/PS 60/40, PVP/PS 10/90, and PVP/PS/PAN 20/70/10, covered

with an electrospun PAN layer (Fig. 1B). We have provided evidence that these dual HLB properties, together with the high surface area and interconnectivity of the open microporous electrospun network, make the MetaSAMP®s' core membranes excellent substrates for the enrichment, desorption and ionization of analytes with a broad physicochemical diversity in terms of characteristics such as size and polarity (*m/z* 100–1200 Da and logP of -4 to 13) (Fig. 2 and fig. S12). Indeed, Bian and Olesik (*41*) already reported that electrospun nanofibrous membranes may serve as an excellent substrate for a selection of small drug molecule analysis because of the nature of their microporous network, while different HLB-based ab- and adsorptive sampling approaches have been described (*28*) which have proven beneficial for subsequent MS-based analysis of a physiochemically broad range of metabolites. In contrast to the rectal and salivary core MetaSAMP® membranes, we found that for the urinary core membrane, a blend of PVP, PS and PAN was most favorable, given the very hydrophilic nature of the waste products that comprise the urinary metabolome (*58*). Indeed, PAN is a polar polymer with wetting capabilities (*33*) that has proven advantageous in diminishing fragmentation and background noise for low molecular masses (*41*). The markedly higher fraction of PS in the salivary and urinary MetaSAMP®s compared to the rectal MetaSAMP®'s composition resulted in a more extensive metabolome coverage, especially for the higher *m/z* ranges in which more lipids reside which are relatively less concentrated and hence more difficult to selectively retain from such polar matrices (*59*). Furthermore, introducing the biocompatible polymer PAN (*34*, *35*) as a cover layer (*29*) reduces biofouling due to restricting access to relatively large (macro)molecules such as DNA and proteins (*29*). Moreover, it facilitates the impregnation of aqueous biofluids into the relatively hydrophobic core layer. Indeed, we observed an increased metabolome recovery and precision upon introduction of an electrospun PAN cover layer. This may be ascribed to the advantageous complementary action of the large (micrometer scale), open pores (*30*) of the core network of the nanofibrous PVP/PS(/PAN) membrane that ad- and absorbs small molecules, and the nanofibrous PAN exclusion layer that prevents the interaction of macromolecules with this nanofibrous network (*29*), most likely resulting in reduced matrix interferences upon LA-REIMS analysis of the MetaSAMP®s. Finally, as also reported by Bian and Olesik, the porosity and very high specific surface area that are inherent to electrospun membranes are especially valuable when coupled to laser-based desorption and ionization (*41*). Indeed, the observation of increased *m/z* signal intensities throughout the different *m/z* mass ranges following MetaSAMP®-LA-REIMS analysis in comparison to crude biofluid LA-REIMS analysis (Fig. 2 and fig. S9) corroborate their findings on fast and efficient energy transfer and dissipation, boosting desorption and ionization when using electrospun nanofibrous substrates (*41*).

The fully optimized biofluid-specific MetaSAMP®s increased the short-term biofluid metabolome stability (at 4°C) and the total sampling and analysis speed. These results point towards a decrease in storage-induced metabolome alterations when using our MetaSAMP®s. Significant salivary and urinary metabolome alterations when storing crude biofluids at 4°C have been reported to occur after 6 hours (*60*) and 5 days (*14*), respectively, confirming our observations. The stabilizing properties of our optimized biofluid-specific MetaSAMP®s are hypothesized to result from the ad- and absorption capabilities of the electrospun fibrous network (*30*) and this both towards the different metabolites present in the biofluid and its aqueous content. In particular, this water content has been shown to provide a means for diverse degradation reactions (oxidation and hydrolysis) and microbial activity (enzymes) (*12*). In line herewith, the gastrointestinal matrices benefited most from MetaSAMP®'s stabilizing effects as an inhibition of the interaction between metabolites and microbes is expected. Moreover, the MetaSAMP®s' protective PAN cover layer also provides a certain degree of shielding of the biofluid metabolites (small molecules) captured via chemical and/or physical interactions (fig. S12) and may hence contribute to this reduced degradation and transformation. Alternative AIMS-based techniques, including other LA-REIMS-based approaches (*1*, *17*), require relatively long collection procedures and/or sample preparation periods that take several hours up to days (*61*). The total analysis time of our optimized biofluid-specific MetaSAMP®-LA-REIMS methodology was <20 min per sample.

We successfully benchmarked the biofluid-specific MetaSAMP®s in the context of a clinically relevant application using samples from two pediatric cohorts (MetaBEAse and OPERA). The ever-increasing rise in overweight and obesity urges the development of cost-effective ways to screen for elevated metabolic risk as early as possible, when metabolic impairments are still reversible (*2*). Our findings provided evidence that MetaSAMP®-based metabotyping enables similarly to superior discriminative categorization of children based on weight classification compared to crude biofluid LA-REIMS analysis (*1*). This was confirmed by high predictive AUC values (>0.9), indicating good to excellent sensitivity and specificity of the metabolic fingerprints sampled and analyzed via MetaSAMP®-LA-REIMS analysis regarding weight classification. Moreover, the obtained metabolic fingerprints exhibited meaningful pathophysiological correlations with a whole range of relevant anthropometric and clinical parameters for (childhood) overweight and obesity. Indeed, the correlations found in this study showed similar (*62*, *63*) or improved (*54*, *63*) Spearman ρ-values (up to 0.5) compared to earlier work. For example, we observed a correlation between the fecal metabolome, BMI and blood lipid levels (Spearman ρ-values of up to 0.4), in line with previous results concerning the fecal metabolome of obese adults (*63*). Similarly, Spearman ρ-values of up to 0.3 for fecal microbiome diversity with BMI and

glycemic and lipid measurements in adults were recently reported (*54*), while our MetaSAMP®s reached ρ-values of up to 0.6 regarding glycemic measurements such as glucose and insulin. In accordance with the literature, we observed that acylcarnitines were positively correlated in children with IOTF>1 and with Waist, WHR and systolic blood pressure (BP), inferring future metabolic risk (*2*). Furthermore, similar positive correlations between anthropometric measurements with 7-ketocholesterol were noted and of clinical relevance as cholesterol derivates are involved in macrophage foam cell formation and thus atherosclerosis (*2*). Finally, we successfully demonstrated the targeted application of our rectal MetaSAMP®-LA-REIMS approach of which the results indicated that potentially clinically relevant fecal metabolites may be detected with acceptable intra-assay and intermediate precision according to FDA recommendations (*56*).

Despite the recent introduction of AIMS in biofluid metabolomics (1, 18), the direct sampling-to-MS result workflow used for these biological matrices still suffers from practical issues such as dependence on sample availability and laboratory pretreatment procedures such as (ultra)centrifugation for protein precipitation. In this aspect, the MetaSAMP® cover layer introduced biocompatibility and reduced biofouling and hence matrix effects due to its selective filtering principle, i.e., hindering relatively large molecules, such as DNA, RNA, and/or proteins from their interaction with the open network of the MetaSAMP®s (fig. S12). Consequently, superior ab- and adsorption for the direct sampling of complex matrices whilst eliminating interfering molecules and facilitating broader (Fig. 2) and more short-term stable (Fig. 3) metabolite recovery was evinced. Indeed, with respect to metabolome coverage (the number of detected metabolic features), our biofluid-specific MetaSAMP®s outperformed what has been previously reported in the literature for AIMS-based metabolomics analysis of human biofluids, including feces (1, 16, 18), saliva (*1*, *13*, *64*) and urine (*1*, *65*, *66*). Our biofluid-specific MetaSAMP®-LA-REIMS methodology provides a promising approach toward the first-line segregation of increased metabolic risk based on distinctive fingerprints that may overcome the limitations of conventional crude biofluid AIMS metabolomics analysis, such as matrix effects. Moreover, biofluid collection, transport and storage are substantially facilitated using our optimized biofluid-specific MetaSAMP®s while supporting the short-term metabolome stability, as such decreasing the possible loss of clinically relevant metabolites in the duration between the home/practitioner's office sampling and laboratory-scale analysis. Rapid high-throughput fingerprinting by MetaSAMP®-LA-REIMS may as such be installed as a prescreening approach, circumventing costly and cumbersome analyses prior to the further in-depth study of discriminative metabolites.

Despite the great clinical opportunities our MetaSAMP®s could bring to the diagnostic, prognostic and/or preventive field of metabolic disease, we do acknowledge some flaws. We have

addressed some (repeatability and reproducibility) but not all typical bioanalytical method validation characteristics, including metabolites' recovery, which has been issued before in studies applying similar principles (*41*, *67–70*), implying the necessity of conventional quantitative hyphenated LC-MS methodologies. Indeed, the main merits of AIMS are high throughput and direct clinical applicability compared to conventional metabolomics platforms. Such advantages have however mainly been restricted to untargeted metabolomics research (*71*) as there still is much to glean from the reproducibility, quantitation exquisiteness and ability to annotate potential differential marker molecules of more dedicated hyphenated analytical platforms (16). Further research is also warranted to longitudinally follow up large-scale cohorts of childhood overweight and obesity to consolidate the potential of MetaSAMP®-based metabotyping as a risk categorization tool in precision medicine. Such longitudinal design will aid to reveal the predictive and/or prognostic value of physiologically relevant differential marker molecules. Furthermore, future work should focus on *in vivo* sampling with the MetaSAMP® to cross-validate the *ex vivo* results presented in this paper.

Materials & Methods

Chemicals and standards

Isopropylalcohol (IPA), methanol (MeOH), and ethanol (EtOH) (all LC–MS-grade) were purchased from Fisher Scientific (UK). N,N-Dimethylformamide (DMF) and chloroform ($CHCl_3$) were purchased from EMPLURA Merck Millipore (BE) and Sigma Aldrich (US), respectively. Ultrapure water (UPW) was obtained through a Sartorius Arium 661 UV water purification system (Millipore, Belgium). Analytical standards (3-hydroxybutyric acid, linoleic acid, L-carnosine, 1,2-dioleoyl-sn-glycero-3-phospho-rac-(1-glycerol) (DOPG), 1-palmitoyl-2-oleoyl-sn-glycero-3-(phospho-rac-(1-glycerol)) (POPG), D-mannitol, myo-inositol, L-cysteine, L-arginine, L-kynurenine and taurolitocholate-3-sulfate) and leucine enkephalin were purchased from Sigma–Aldrich (US), ICN Biomedicals Inc. (US), TLC Pharmchem (CA), or Waters Corporation (US) or as reported in (*11, 72*). Information on the purchased polymers and initial evaluation of different polymer solutions is given under note S1.

Electrospinning

PVP and PS were dissolved in DMF and $CHCl_3$ (1:2, *v/v*) and stirred for a minimum of 4 h at 60°C to obtain a clear solution. PAN (MW=150,000 g/mol, Sigma Aldrich, US) was dissolved in DMF at 5, 8, 10, 12 and 15% (*w/w*), by stirring for a minimum of 2 h at RT and subsequently 1

hour at 90°C until a clear, pale-yellow solution was obtained. The polymer blends (PVP/PS) were loaded in a 20 mL syringe and fed through a syringe KD Scientific KDS-100-CE Pump Series 100 (Sigma Aldrich, US) using a capillary 18G needle of 0.80 mm inner diameter at a flow rate of 1 mL h^{-1} and 1.5 mL min^{-1} for the core (PVP/PS for the salivary and rectal MetaSAMP® and PVP/PS-PAN for the urinary MetaSAMP®) and PAN cover layers, respectively. A Glassman High Voltage Series EH (High Bridge, US) was clamped to the tip of the needle and was used to apply a voltage between 15-17.5 kV. The tip-to-collector distance was averaged at 15 cm but slightly altered during the ES process towards attaining a stable, *i.e.*, steady-state, Taylor cone (*73*). The nanofibrous network was collected on a grounded, thick aluminium foil-covered metal drum collector (Linari NanoTech, Italy) rotating at 125 RPM. All experiments were performed at ambient conditions, *i.e.*, RT (22±2°C) and relative humidity (RH) of 30±10%, in a fumehood (*73*). MDSC measurements were performed (fig. S3) to determine the Tg of the polymers in the blend. Specifications of the viscosity measurements, SEM analyses, mDSC method, and CAMs are elaborated under note S2.

LA-REIMS instrumental analysis

All LA-REIMS analyses were performed using our previously biofluid-specific optimized protocols for urine and saliva (*1*), while for the rectal MetaSAMP®-LA-REIMS analysis the protocol was optimized using a DOE design as described in note S3.1. The final optimized parameters are described in table S1. A mid-IR laser system (Opolette 2940, Opotek, US) was used as a desorption and ionization source hyphenated by a PTFE aerosol channeling tube to a Xevo G2-XS quadrupole time-of-flight (Q-ToF) mass spectrometer (Waters Corporation, US). A more comprehensive description of the instrumental analysis is described under note S3.2. LA-REIMS analysis of MetaSAMP®s and crude biofluids was performed using our custom-built platform according to the manual and fully automated methodology, respectively, as described by Plekhova (1) (note S3.3).

Clinical study samples

Fresh feces (Fecotainer®, Excretas Medical BV, NL) and urine (6-12 years, Metabolomics research on Early Metabolic Disease (MetaBEAse) cohort, ClinicalTrials.gov (NCT04632511)) and saliva (6–16 years, Obesity Prevention through Emotion Regulation in Adolescents (OPERA) cohort (*42*)) were collected. The Ghent University Hospital Ethics Committee approved both studies (BC-06939 and EC 2016/0673) and informed consent was obtained from every participant and their caretakers. Samples were stored at -80°C following collection and thawed at RT (22±2°C)

before analysis. Participant fecal samples underwent lyophilization (Christ 1-4 Alpha LSC*plus*), resulting in an average removal of 55.9%±6.4% water. Saliva samples were pretreated as described previously (*13*), and urine samples were used after thawing without additional processing.

The study participants were of both sexes (Table 1), were pseudonymized, and did not receive antibiotic treatment for at least three months before sample donation or take any long-term medication (*72*). The classification was performed based on BMI *z*-scores (adjusted BMI for age and sex) (*74*) and IOTF score (*75*).

Sample preparation for optimization and short-term stability experiments

For initial optimization experiments with the rectal MetaSAMP®, rectal sampling was mimicked by impregnating pieces (ca. 1 x 1 cm) of the electrospun PVP/PS membranes with the contents of freshly collected porcine colon and rectum (EC2018_70 and EC2018_91, Ghent University, Department of Translational Physiology, Infectiology and Public Health, Merelbeke, BE). For the primary experiments with the salivary and urinary MetaSAMP®, sampling was performed using pooled QC samples (*N*=6) (UGent-LCA biobank 210016). To evaluate the short-term stability of the rectal, salivary and urinary MetaSAMP®s nanofiber composition, remaining aliquots from the samples of our MetaBEAse and OPERA pediatric cohorts (*N*=6 for each biofluid) were combined to create pooled QC samples that aimed to reflect inherent biological variation. Pooled QC samples of the 3 biofluids were used to maximize metabolite coverage without substantially increasing the number of analyses (*12*, *76*).

For the pooled QC samples used during optimization and short-term stability experiments, fecal water was prepared by the addition of UPW to the fresh fecal sample at a 1:4 ratio (*w/v %*) followed by homogenization (Stomacher 400, Seward, Worthing, UK) for 10 min at the highest intensity (*77*) (see also note S5, fig. S19 and table S11) and subsequent centrifugation (Rotanta 460R, Hettich Zentrifugen, DE) at RT (500 x *g*, 2 min). The collected supernatant was divided into aliquots, which were stored at -80°C. As such, freeze–thaw cycling, which may negatively affect metabolome stability (*12*), was limited since a new aliquot was used, after thorough vortexing (1 min at 400 x *g*, IKA vortex 3, IKA, DE), for every optimization experiment performed. In line with the optimization (note S1.3), electrospun membrane pieces (ca. 1 x 1 cm in size, matching the dimensions of a 24-well plate (Greiner CELLSTAR, Greiner Bio One, DE)) were spiked with 30 µL of fecal water, saliva or urine and impregnated for 10-15 min. For direct biofluid analysis (*i.e.*, without MetaSAMP® impregnation), 100 µL of each sample was added to a 96-well plate (Greiner 96-well microplates, Greiner Bio One, DE).

Compositional optimization, short-term stability, and laser ablation interaction evaluation of the biofluid-specific MetaSAMP®s

The ratios at which PVP and PS were blended were controlled by varying the relative weight ratios of each polymer as well as the polymer weight relative to the total solution weight (*w/w*). Moreover, the addition of the PAN top layer (5-15%, *w/w*) was examined through the quality of the fiber network by SEM and evaluated in terms of metabolome coverage. To this end, both DOE matrices and response surface methodology (RSM) models were constructed with the software program Modde™ (Sartorius, DE), whereby the compositions (polymer ratio (PVP%, *w/w*), polymer weight% (*w/w*)), duration of spinning the PAN cover layer (min) and duration of spinning the core membrane (h) for the rectal MetaSAMP® (table S5 and fig. S13A-C) and polymer ratio (PVP%, *w/w*), presence of PAN in the polymer blend (%), duration of spinning the PAN cover layer (min) and duration of spinning the core membrane (h) for the salivary and urinary MetaSAMP®s were evaluated (table S6 and fig. S13D-I). The goal was to maximize metabolome coverage, measurement repeatability (*N*=5) (*72*), summarized normalized LA-REIMS intensity (*78*) and obtain good quality of the fiber network (by inspecting SEM images). Subsequently, the number of molecular features covered and their relative number (%) with CV ≤30% (*72*) were compared.

A short-term stability study of the impregnated optimized rectal, salivary and urinary MetaSAMP®s was performed by using QC pool samples (see above) for up to 48 h at RT (22±2°C) and 4°C. As described above, biofluids were either applied on the respective MetaSAMP® surface or analyzed as such directly upon collection (first timepoint) and after storage (second time point). For each condition 8 sample aliquots were analyzed, of which 3 replicate measurements were performed.

In addition, to assure reliable metabolome investigation following the application of LA-REIMS onto electrospun polymer networks, the interaction between substrate and analytical beam, *i.e.*, the optimized MetaSAMP®s and laser upon ablation, respectively, was assessed (note S4 and fig. S16-S17).

Analytical and biological validation of the MetaSAMP®-LA-REIMS methodology

The optimized MetaSAMP® configurations were subjected to analytical (targeted and untargeted) and biological (untargeted) validation. To this end, feces and urine from children (MetaBEAse cohort, *N*=88, IOTF≥1 and *N*=146, IOTF<1) and saliva samples from children

(OPERA cohort (*42*), *N*=66, IOTF=0, *N*=29 IOTF≥1) (*13*) were impregnated under the same experimental conditions as described above onto the optimized electrospun membranes.

The instrumental, intra-assay precision or repeatability, and intermediate precision of the MetaSAMP®-LA-REIMS methodology was assessed to confirm the analytical method as fit-for-purpose according to FDA recommendations (*11*, *56*). This is, technical repeatability was assessed by LA-REIMS automated analysis (*N*=3 burns of the same sample) (*1*) of the pooled QC samples and standard mixtures. For the intra-assay and intermediate precision tests, 5 pieces from an electrospun membrane were analyzed under repeatable experimental conditions by the same operator, and this setup was used again on a different day by another operator, respectively.

The target analytes (30 µL at 100 ng μL^{-1}) were spiked using a micropipette onto the rectal MetaSAMP® membranes in solvent (UPW and IPA, according to logP of the target analytes) as well as in fecal water into a 24-well plate (Greiner CELLSTAR, Greiner Bio One, DE) and subjected to our automatic platform for LA-REIMS analysis (*1*). The mass spectra generated in MassLynx™ and through our in-house data analysis pipeline as well as mass accuracy data for both platforms were investigated, and the repeatability of the targeted analysis was examined using the CV values. For this purpose, we evaluated the accurate *m/z* values of detectable adducts of the molecular ions to three decimal places after mass drift correction (LA-REIMS data and the monoisotopic mass from HMDB (*57*)).

To assess the applicability of the MetaSAMP®-LA-REIMS platform, the established methodology was implemented in the clinical context of pediatric overweight and obesity (see above). The associations between anthropometric and clinical and metabolic blood data with molecular features were computed in those two independent cohorts (MetaBEAse and OPERA (*42*) cohorts) using Spearman's rank correlation analysis (*54*) (absolute correlation values or moduli reported with ρ) and corresponding *p*-values (Wilcoxon rank-sum tests with continuity correction) for each pair of metadata and molecular feature under investigation.

Ultrahigh-performance liquid chromatography coupled to HRMS analysis, a more comprehensive analysis technique that is conventionally used in metabolomics research (Tiers 1-3 according to metabolite identification standards (*76*)), was addressed to enable metabolite annotation of potentially clinically relevant molecular features. For this purpose, a selection of representative crude fecal patient samples (*N*=4, extracted fecal samples of obese children (IOTF>1), MetaBEAse cohort) and 525 fecal in-house analytical standards (data S7) were analyzed accordingly by combined complementary metabolomics (*11*) and lipidomics (*72*) analysis.

For every validation experiment, a pool of randomly selected clinical cohort samples ($n \geq 20$) was prepared to include as QC sample during analysis to monitor instrument performance. For this

purpose, QC samples were included at the beginning and end of the analytical batch (*N*=6), as well as during analysis (*N*=2) after every 10 samples, and samples were analyzed in a randomized order.

Data and statistical analysis

LA-REIMS molecular fingerprints were acquired by MassLynx™ (version 4.2, Waters, Corporation, US, stored as raw directories). To counteract plausible time-dependent instrumental variability, lock mass correction against the *m/z* value of leucine enkephalin (554.262 Da for negative ion mode data, 100 mDa mass tolerance window) was performed. Data were preprocessed to select representative burns and perform peak picking using Progenesis® Bridge (version 1.0.29) and Progenesis® QI (version 2.3., Waters Corporation, US), respectively, as described previously (1). Progenesis® Bridge preprocesses the original raw data, acquired using the LA-REIMS set-up, into bridged data by adaptive background subtraction according to the sample-specific total ion current (TIC) replicate threshold specified (applied thresholds of 2 e^6 to 5 e^7, depending on the experiments performed). Progenesis® QI applies a peak-picking algorithm and performs TIC normalization, resulting in lists of *m/z* features. Further data analyses were conducted using R (version 3.4.3, AT) and Python (version 3.7.4, US) (table S12). Preprocessed data were subjected to pretreatment optimization, including a range of tested normalization strategies, which included QC-based robust locally estimated scatterplot smoothing signal correction (QC-RLSC algorithm) (*13*), internal QC correction, and TIC correction as well as their combinations. Molecular features, as addressed in terms of feature count and % of features below CV threshold, were assigned as relevant only when they occurred in at least 80% of QC replicates. For intensity analysis and the evaluation of replicate measures, mean, SD and CV values were calculated. All multivariate models were built using SIMCA® (Sartorius, DE) after selection of the best raw data pretreatment strategy and the associated data. Unsupervised principal component analysis (PCA) was used for the identification of outliers, the evaluation of instrument stability based on QC clustering, and the assessment of the natural patterning of samples according to inherent metabolic fingerprints. Supervised multivariate statistical modeling using OPLS-DA was performed to assess the discriminative and predictive performance of the metabolic fingerprints. Additionally, receiver operator characteristic (ROC) analysis of the fecal and urinary metabolome coverage (MetaBEAse cohort) was executed based on the logistic regression classification model (75-25 train-test split after balancing data, performed using five-fold cross-validation). Logistic regression is a popular method to analyze injury case-control studies, and has some advantages over linear regression analysis, using maximum likelihood estimation methods. To optimize the predictive power of our models, molecular features (1750 in

total) were iteratively eliminated from the dataset while monitoring the accuracy of models trained on this reduced dataset. Quantification of AUC values and corresponding 95% CI was performed using bootstrap resampling (N=200). To perform the Spearman correlation analysis, normalized, log-transformed and Pareto scaled datasets were used. In addition, univariate Wilcoxon rank-sum tests with continuity correction were performed with the normalized dataset (rectal MetaSAMP®) to study which molecular features showed good and significant (p<0.05) correlations with anthropometric and/or clinical parameters. Regarding the latter, the Spearman ρ-values were ranked based on their moduli to select the highest correlations. However, for the clinical evaluation of the metabolite's positive or negative correlation with a specific parameter, the signs of Spearman ρ-values were considered. Targeted data processing of the significant molecular features was carried out with Xcalibur™ 3.0 software (Thermo Fisher Scientific, US), whereby compounds were identified based on their *m/z* value, C-isotope profile, and retention time relative to that of the internal standard, followed by putative identification (*76*) of significant and highly correlated LA-REIMS-MetaSAMP® features (mass deviation below 50 ppm). Pairwise univariate and multiple comparisons were evaluated for the identified molecular features according to different IOTF groups based on Wilcoxon rank-sum test with continuity correction and Kruskal–Wallis test with Dunn's post-hoc test, respectively.

The R language was also used for preprocessing, data handling, and statistical analysis of data from the targeted analysis of spiked analytes representing clinically relevant metabolites in (childhood) overweight and obesity (*2*) with varying physicochemical properties (mass error tolerance set at a maximum value of 150 ppm), including a visualization tool generating mass spectra and graphics (data S8).

References

1. V. Plekhova, L. Van Meulebroek, M. De Graeve, A. Perdones-montero, M. De Spiegeleer, E. De Paepe, E. Van De Walle, Z. Takats, S. J. S. Cameron, L. Vanhaecke, Rapid ex vivo molecular fingerprinting of biofluids using laser-assisted rapid evaporative ionization mass spectrometry. *Nat. Protoc.* **16**, 4327–4354 (2021).
2. M. De Spiegeleer, E. De Paepe, L. Van Meulebroek, I. Gies, J. De Schepper, L. Vanhaecke, Paediatric obesity: a systematic review and pathway mapping of metabolic alterations underlying early disease processes. *Mol. Med.* **27**, 1–20 (2021).
3. G. F. Giskeodegard, S. K. Davies, V. L. Revell, H. Keun, D. J. Skene, Diurnal rhythms in the human urine metabolome during sleep and total sleep deprivation. *Sci. Rep.* **5**, 1–11 (2015).
4. M. McEniry, Early-life conditions and older adult health in low- and middle-income countries: A review. *J. Dev. Orig. Health Dis.* **4**, 10–29 (2013).
5. N. Liu, J. Xiao, C. Gijavanekar, K. L. Pappan, K. E. Glinton, B. J. Shayota, A. D. Kennedy, Q. Sun, V. R. Sutton, S. H. Elsea, Comparison of Untargeted Metabolomic Profiling vs Traditional Metabolic Screening to Identify Inborn Errors of Metabolism.

JAMA Netw. Open. **4**, 1–14 (2021).
6. World Health Organization, “Who European Regional Obesity Report 2022” (2022).
7. R. L. Rosenfield, CLINICAL REVIEW: Identifying Children at Risk for Polycystic Ovary Syndrome. *J. Clin. Endocrinol. Metab.* **92**, 787–796 (2007).
8. A. Deeb, S. Attia, S. Mahmoud, G. Elhaj, A. Elfatih, Dyslipidemia and Fatty Liver Disease in Overweight and Obese Children. *J. Obes.*, 1–6 (2018).
9. D. C. Masquio, A. eP. Ganen, R. M. Campos, P. eL. Sanches, F. C. Corgosinho, D. Caranti, L. Tock, M. T. de Mello, S. Tufik, A. R. Dâmaso, Cut-off values of waist circumference to predict metabolic syndrome in obese adolescents. *Nutr. Hosp.* **31**, 1540–1550 (2015).
10. M. Propst, C. Colvin, R. L. Griffin, B. Sunil, C. M. Harmon, G. Yannam, J. E. Johnson, C. B. Smith, A. P. Lucas, B. T. Diaz, A. P. Ashraf, Diabetes and prediabetes are significantly higher in morbidly obese children compared with obese children. *Endocr. Pract.* **21**, 1046–1053 (2015).
11. E. De Paepe, L. Van Meulebroek, C. Rombouts, S. Huysman, K. Verplanken, B. Lapauw, J. Wauters, L. Y. Hemeryck, L. Vanhaecke, A validated multi-matrix platform for metabolomic fingerprinting of human urine, feces and plasma using ultra-high performance liquid-chromatography coupled to hybrid orbitrap high-resolution mass spectrometry. *Anal. Chim. Acta*. **1033**, 108–118 (2018).
12. M. De Spiegeleer, M. De Graeve, S. Huysman, A. Vanderbeke, L. Van Meulebroek, L. Vanhaecke, Impact of storage conditions on the human stool metabolome and lipidome : Preserving the most accurate fingerprint. *Anal. Chim. Acta*. **1108**, 79–88 (2020).
13. K. Wijnant, L. Van Meulebroek, B. Pomian, K. De Windt, S. De Henauw, N. Michels, L. Vanhaecke, Validated Ultra-High-Performance Liquid Chromatography Hybrid High-Resolution Mass Spectrometry and Laser-Assisted Rapid Evaporative Ionization Mass Spectrometry for Salivary Metabolomics. *Anal. Chem.* **92**, 5116–5124 (2020).
14. J. Laparre, Z. Kaabia, M. Mooney, T. Buckley, M. Sherry, B. Le Bizec, G. Dervilly-Pinel, Impact of storage conditions on the urinary metabolomics fingerprint. *Anal. Chim. Acta*. **951**, 99–107 (2016).
15. W. Lu, X. Su, M. S. Klein, I. A. Lewis, O. Fiehn, J. D. Rabinowitz, Metabolite Measurement: Pitfalls to Avoid and Practices to Follow. *Annu. Rev. Biochem.* **86**, 277–304 (2017).
16. L. Van Meulebroek, S. Cameron, V. Plekhova, M. De Spiegeleer, K. Wijnant, N. Michels, S. De Henauw, B. Lapauw, L. Vanhaecke, Rapid LA-REIMS and comprehensive UHPLC-HRMS for metabolic phenotyping of feces. *Talanta*. **217**, 1–9 (2020).
17. P. Pruski, D. A. MacIntyre, H. V. Lewis, P. Inglese, G. D. S. Correia, T. T. Hansel, P. R. Bennett, E. Holmes, Z. Takats, Medical Swab Analysis Using Desorption Electrospray Ionization Mass Spectrometry: A Noninvasive Approach for Mucosal Diagnostics. *Anal. Chem.* **89**, 1540–1550 (2017).
18. S. J. S. Cameron, J. L. Alexander, F. Bolt, A. Burke, H. Ashrafian, J. Teare, J. R. Marchesi, J. Kinross, J. V. Li, Z. Takáts, Evaluation of Direct from Sample Metabolomics of Human Feces Using Rapid Evaporative Ionization Mass Spectrometry. *Anal. Chem.* **91**, 13448–13457 (2019).
19. X. Li, R. Xu, X. Wei, H. Hu, S. Zhao, Y. M. Liu, Direct Analysis of Biofluids by Mass Spectrometry with Microfluidic Voltage-Assisted Liquid Desorption Electrospray Ionization. *Anal. Chem.* **89**, 12014–12022 (2017).
20. B. Fatou, P. Saudemont, E. Leblanc, D. Vinatier, V. Mesdag, M. Wisztorski, C. Focsa, M. Salzet, M. Ziskind, I. Fournier, In vivo Real-Time Mass Spectrometry for Guided Surgery Application. *Sci. Rep.* **6**, 1–14 (2016).
21. N. Abbassi-Ghadi, E. A. Jones, M. Gomez-Romero, O. Golf, S. Kumar, J. Huang, H.

Kudo, R. D. Goldin, G. B. Hanna, Z. Takats, A Comparison of DESI-MS and LC-MS for the Lipidomic Profiling of Human Cancer Tissue. *J. Am. Soc. Mass Spectrom.* **27**, 255–264 (2016).
22. A. Alonso, S. Marsal, A. JuliÃ, Analytical Methods in Untargeted Metabolomics: State of the Art in 2015. *Front. Bioeng. Biotechnol.* **3**, 1–20 (2015).
23. T. H. Kuo, E. P. Dutkiewicz, J. Pei, C. C. Hsu, Ambient Ionization Mass Spectrometry Today and Tomorrow: Embracing Challenges and Opportunities. *Anal. Chem.* **92**, 2353–2363 (2020).
24. J. Geltmeyer, L. Van Der Schueren, F. Goethals, K. De Buysser, K. De Clerck, Optimum sol viscosity for stable electrospinning of silica nanofibres. *J. Sol-Gel Sci. Technol.* **67**, 188–195 (2013).
25. M. S. Islam, B. C. Ang, A. Andriyana, A. M. Afifi, A review on fabrication of nanofibers via electrospinning and their applications. *SN Appl. Sci.* **1**, 1–16 (2019).
26. N. Reyes-Garcés, E. Gionfriddo, G. A. Gómez-Ríos, M. N. Alam, E. Boyacl, B. Bojko, V. Singh, J. Grandy, J. Pawliszyn, Advances in Solid Phase Microextraction and Perspective on Future Directions. *Anal. Chem.* **90**, 302–360 (2018).
27. T. Lu, S. V Olesik, Electrospun Nanofibers as Substrates for Surface-Assisted Laser Desorption/Ionization and Matrix-Enhanced Surface-Assisted Laser Desorption/Ionization Mass Spectrometry. *Anal. Chem.* **85**, 4384–4391 (2013).
28. E. Gionfriddo, E. Boyacl, J. Pawliszyn, New Generation of Solid-Phase Microextraction Coatings for Complementary Separation Approaches: A Step toward Comprehensive Metabolomics and Multiresidue Analyses in Complex Matrices. *Anal. Chem.* **89**, 4046–4054 (2017).
29. B. Onat, H. Rosales-Solano, J. Pawliszyn, Development of a Biocompatible Solid Phase Microextraction Thin Film Coating for the Sampling and Enrichment of Peptides. *Anal. Chem.* **92**, 9379–9388 (2020).
30. T. Meireman, L. Daelemans, S. Rijckaert, H. Rahier, W. Van Paepegem, K. De Clerck, Delamination resistant composites by interleaving bio-based long-chain polyamide nanofibers through optimal control of fiber diameter and fiber morphology. *Compos. Sci. Technol.* **193**, 1–10 (2020).
31. K. L. Nielsen, M. L. Hartvigsen, M. S. Hedemann, H. N. Lræke, K. Hermansen, K. E. Bach Knudsen, Similar metabolic responses in pigs and humans to breads with different contents and compositions of dietary fibers: A metabolomics study. *Am. J. Clin. Nutr.* **99**, 941–949 (2014).
32. S. Huysman, F. Vanryckeghem, E. De Paepe, F. Smedes, S. A. Haughey, C. T. Elliott, K. Demeestere, L. Vanhaecke, Hydrophilic Divinylbenzene for Equilibrium Sorption of Emerging Organic Contaminants in Aquatic Matrices. *Environ. Sci. Technol.* **53**, 10803–10812 (2019).
33. P. Franco, I. De Marco, The Use of Poly(N-vinyl pyrrolidone) in the Delivery of Drugs: A Review. *Polymers (Basel).* **12**, 1–29 (2020).
34. X. Liu, T. Lin, J. Fang, G. Yao, H. Zhao, M. Dodson, X. Wang, In vivo wound healing and antibacterial performances of electrospun nanofibre membranes. *J Biomed Mater Res A.* **94**, 499–508 (2010).
35. J. Xue, T. Wu, Y. Dai, Y. Xia, Electrospinning and electrospun nanofibers: Methods, materials, and applications. *Chem. Rev.* **119** (2019), pp. 5298–5415.
36. J. Niska-Blakie, L. Gopinathan, K. N. Low, Y. L. Kien, C. M. F. Goh, M. J. Caldez, E. Pfeiffenberger, O. S. Jones, C. B. Ong, I. V Kurochkin, V. Coppola, L. Tessarollo, H. Choi, Y. Kanagasundaram, F. Eisenhaber, S. Maurer-Stroh, P. Kaldis, Knockout of the non-essential gene SUGCT creates diet-linked, age-related microbiome disbalance with a diabetes-like metabolic syndrome phenotype. *Cell. Mol. Life Sci.* **77**, 3423–3439 (2020).

37. M. Reyman, M. A. van Houten, K. Arp, E. A. M. Sanders, D. Bogaert, Rectal swabs are a reliable proxy for faecal samples in infant gut microbiota research based on 16S-rRNA sequencing. *Sci. Rep.* **9**, 1–8 (2019).
38. R. B. Jones, X. Zhu, E. Moan, H. J. Murff, R. M. Ness, D. L. Seidner, S. Sun, C. Yu, Q. Dai, A. A. Fodor, M. A. Azcarate-Peril, M. J. Shrubsole, Inter-niche and inter-individual variation in gut microbial community assessment using stool, rectal swab, and mucosal samples. *Sci. Rep.* **8**, 1–12 (2018).
39. E. A. Jones, D. Simon, T. Karancsi, J. Balog, S. D. Pringle, Z. Takats, Matrix assisted rapid evaporative ionization mass spectrometry. *Anal. Chem.* **91**, 9784–9791 (2019).
40. P. T. Ivanova, S. B. Milne, H. A. Brown, Identification of atypical ether-linked glycerophospholipid species in macrophages by mass spectrometry. *J. Lipid Res.* **51**, 1581–1590 (2010).
41. J. Bian, S. V. Olesik, Surface-assisted laser desorption/ionization time-of-flight mass spectrometry of small drug molecules and high molecular weight synthetic/biological polymers using electrospun composite nanofibers. *Analyst*. **142**, 1125–1132 (2017).
42. K. Wijnant, J. Klosowska, C. Braet, S. Verbeken, S. De Henauw, L. Vanhaecke, N. Michels, J.-B. Bouillon-Minois, Stress Responsiveness and Emotional Eating Depend on Youngsters' Chronic Stress Level and Overweight Academic Editors: Frederic Dutheil. *Nutrients*. **13**, 1–16 (2021).
43. I. Agueusop, P. B. Musholt, B. Klaus, K. Hightower, A. Kannt, Short-term variability of the human serum metabolome depending on nutritional and metabolic health status. *Sci. Rep.* **10**, 1–13 (2020).
44. E. De Paepe, L. Van Gijseghem, M. De Spiegeleer, E. Cox, L. Vanhaecke, A Systematic Review of Metabolic Alterations Underlying IgE-Mediated Food Allergy in Children. *Mol. Nutr. Food Res.* **2100536**, 1–12 (2021).
45. J. D. Blume, Bounding Sample Size Projections for the Area Under a ROC Curve. *J Stat Plan Inference*. **139**, 711–721 (2009).
46. E. Chavira-Suarez, C. Rosel-Pech, E. Polo-Oteyza, M. Ancira-Moreno, I. Ibarra-Gonzalez, M. Vela-Amieva, N. Meraz-Cruz, C. Aguilar-Salinas, F. Vadillo-Ortega, Simultaneous evaluation of metabolomic and inflammatory biomarkers in children with different body mass index (BMI) and waist-to-height ratio (WHtR). *PLoS One*. **15**, 1–13 (2020).
47. P. Schober, L. A. Schwarte, Correlation coefficients: Appropriate use and interpretation. *Anesth. Analg.* **126**, 1763–1768 (2018).
48. American diabetes association, 2. Classification and diagnosis of diabetes: Standards of medical care in diabetesd2019. *Diabetes Care*. **42**, S13–S28 (2019).
49. M. Ramon-Krauel, M. J. Leal-Witt, Ó. Osorio-Conles, M. Amat-Bou, C. Lerin, D. M. Selva, Relationship between adiponectin, TNFα, and SHBG in prepubertal children with obesity. *Mol. Cell. Pediatr.* **8**, 1–6 (2021).
50. R. Santos-Silva, M. Fontoura, J. T. Guimarães, H. Barros, A. C. Santos, Association of dehydroepiandrosterone sulfate, birth size, adiposity and cardiometabolic risk factors in 7-year-old children. *Pediatr. Res.* **91**, 1897–1905 (2021).
51. M. D. Klok, S. Jakobsdottir, M. L. Drent, The role of leptin and ghrelin in the regulation of food intake and body weight in humans: a review. *Obes. Rev.* **8**, 21–34 (2007).
52. A.-V. Sitar-Taut, A. Cozma, A. Fodor, S.-C. Coste, O. H. Orasan, V. Negrean, D. Pop, D.-A. Sitar-Taut, New Insights on the Relationship between Leptin, Ghrelin, and Leptin/Ghrelin Ratio Enforced by Body Mass Index in Obesity and Diabetes. *Biomedicines*. **9**, 1–15 (2021).
53. R. Liu, J. Hong, X. Xu, Q. Feng, D. Zhang, Y. Gu, J. Shi, S. Zhao, W. Liu, X. Wang, H. Xia, Z. Liu, B. Cui, P. Liang, L. Xi, J. Jin, X. Ying, X. Wang, X. Zhao, W. Li, H. Jia, Z. Lan, F. Li, R. Wang, Y. Sun, M. Yang, Y. Shen, Z. Jie, J. Li, X. Chen, H. Zhong, H. Xie,

Y. Zhang, W. Gu, X. Deng, B. Shen, X. Xu, H. Yang, G. Xu, Y. Bi, S. Lai, J. Wang, L. Qi, L. Madsen, J. Wang, G. Ning, K. Kristiansen, W. Wang, Gut microbiome and serum metabolome alterations in obesity and after weight-loss intervention. *Nat. Med.* **23**, 859–868 (2017).
54. F. Asnicar, A. T. Chan, C. Huttenhower, T. D. Spector, N. Segata, S. E. Berry, A. M. Valdes, L. H. Nguyen, G. Piccinno, D. A. Drew, E. Leeming, R. Gibson, C. Le Roy, H. Al Khatib, L. Francis, M. Mazidi, O. Mompeo, M. Valles-Colomer, A. Tett, F. Beghini, L. Dubois, D. Bazzani, A. Maltez Thomas, C. Mirzayi, A. Khleborodova, S. Oh, R. Hine, C. Bonnett, J. Capdevila, S. Danzanvilliers, F. Giordano, L. Geistlinger, L. Waldron, R. Davies, G. Hadjigeorgiou, J. Wolf, J. M. Ordovás, Microbiome connections with host metabolism and habitual diet from 1,098 deeply phenotyped individuals. *Nat. Med.* **27**, 321–332 (2021).
55. M. Mar Rodríguez, D. Pérez, F. J. Chaves, E. Esteve, P. Marin-Garcia, G. Xifra, J. Vendrell, M. Jové, R. Pamplona, W. Ricart, M. Portero-Otin, M. R. Chacón, J. Manuel Fernández Real, Obesity changes the human gut mycobiome. *Sci. reportsts*. **5** (2015).
56. Food and Drug Administration (FDA), Guidance for Industry: Bioanalytical Method Validation (2018) (available at https://www.fda.gov/downloads/drugs/guidances/ucm070107.Pdf).
57. D. S. Wishart, A. Guo, E. Oler, F. Wang, A. Anjum, H. Peters, R. Dizon, Z. Sayeeda, S. Tian, B. L. Lee, M. Berjanskii, R. Mah, M. Yamamoto, J. Jovel, C. Torres-Calzada, M. Hiebert-Giesbrecht, V. W. Lui, D. Varshavi, D. Varshavi, D. Allen, D. Arndt, N. Khetarpal, A. Sivakumaran, K. Harford, S. Sanford, K. Yee, X. Cao, Z. Budinski, J. Liigand, L. Zhang, J. Zheng, R. Mandal, N. Karu, M. Dambrova, H. B. Schï Oth, R. Greiner, V. Gautam, HMDB 5.0: the Human Metabolome Database for 2022. *Nucleic Acids Res.* **50** (2022).
58. S. Bouatra, F. Aziar, A. Mandal, R, Chi Guo, R. M. Wilson, The Human Urine Metabolome. *PLoS One*. **8** (2013).
59. Tipthara Phornpimon, T. Visith, "Chapter 7: Urinary Lipidomics" in *Translational Bioinformatics 14: Lipidomics in Health & Disease* (2018), vol. 14, pp. 97–112.
60. D. Duarte, B. Castro, J. Pereira, J. Marques, A. Costa, A. Gil, Evaluation of Saliva Stability for NMR Metabolomics: Collection and Handling Protocols. *Metabolites*. **10**, 1–15 (2020).
61. T. Vasiljevic, G. A. Gómez-Ríos, J. Pawliszyn, Single-Use Poly(etheretherketone) Solid-Phase Microextraction-Transmission Mode Devices for Rapid Screening and Quantitation of Drugs of Abuse in Oral Fluid and Urine via Direct Analysis in Real-Time Tandem Mass Spectrometry. *Anal. Chem.* **90**, 952–960 (2018).
62. S. Liang, Z. Hou, X. Li, J. Wang, L. Cai, R. Zhang, J. Li, The fecal metabolome is associated with gestational diabetes mellitus. *RSC Adv.* **9**, 29973–29979 (2019).
63. M. Cui, A. Trimigno, J. L. Castro-Mejía, S. Reitelseder, J. Bülow, R. L. Bechshøft, D. S. Nielsen, L. Holm, S. B. Engelsen, B. Khakimov, Human fecal metabolome reflects differences in body mass index, physical fitness, and blood lipoproteins in healthy older adults. *Metabolites*. **11**, 1–16 (2021).
64. X. Song, H. Chen, R. N. Zare, Conductive Polymer Spray Ionization Mass Spectrometry for Biofluid Analysis. *Anal. Chem.* **90**, 12878–12885 (2018).
65. F. G. Pinto, I. Mahmud, T. A. Harmon, V. Y. Rubio, T. J. Garrett, Rapid Prostate Cancer Noninvasive Biomarker Screening Using Segmented Flow Mass Spectrometry-Based Untargeted Metabolomics. *J. Proteome Res.* **19**, 2080–2091 (2020).
66. J. Zhang, T. Fuhrer, H. Ye, B. Kwan, D. Montemayor, J. Tumova, M. Darshi, F. Afshinnia, J. J. Scialla, A. Anderson, A. C. Porter, J. J. Taliercio, H. Rincon-Choles, P. Rao, D. Xie, H. Feldman, U. Sauer, K. Sharma, L. Natarajan, High-Throughput Metabolomics and Diabetic Kidney Disease Progression: Evidence from the Chronic Renal Insufficiency

(CRIC) Study. *Am. J. Nephrol.* **53**, 215–225 (2022).
67. P. Pruski, G. D. S. Correia, H. V. Lewis, K. Capuccini, P. Inglese, D. Chan, R. G. Brown, L. Kindinger, Y. S. Lee, A. Smith, J. Marchesi, J. A. K. McDonald, S. Cameron, K. Alexander-Hardiman, A. L. David, S. J. Stock, J. E. Norman, V. Terzidou, T. G. Teoh, L. Sykes, P. R. Bennett, Z. Takats, D. A. MacIntyre, Direct on-swab metabolic profiling of vaginal microbiome host interactions during pregnancy and preterm birth. *Nat. Commun.* **12**, 1–14 (2021).
68. A. McCarthy, L. Saldana, D. N. Ackerman, Y. Su, J. V. John, S. Chen, S. Weihs, S. P. Reid, J. L. Santarpia, M. A. Carlson, J. Xie, Ultra-absorptive Nanofiber Swabs for Improved Collection and Test Sensitivity of SARS-CoV-2 and other Biological Specimens. *Nano Lett.* **21**, 1508–1516 (2021).
69. T. Gaissmaier, M. Siebenhaar, V. Todorova, V. Hüllen, C. Hopf, Therapeutic drug monitoring in dried blood spots using liquid microjunction surface sampling and high resolution mass spectrometry. *Analyst*. **141**, 892–901 (2016).
70. C. Vega, C. Spence, C. Zhang, B. J. Bills, N. E. Manicke, Ionization Suppression and Recovery in Direct Biofluid Analysis Using Paper Spray Mass Spectrometry. *J. Am. Soc. Mass Spectrom.* **27**, 726–734 (2016).
71. J. D. Odom, R. V. Sutton, Metabolomics in Clinical Practice: Improving Diagnosis and Informing Management. *Clin. Chem.* **12**, 1–12 (2021).
72. L. Van Meulebroek, E. De Paepe, V. Vercruysse, B. Pomian, S. Bos, B. Lapauw, L. Vanhaecke, Holistic Lipidomics of the Human Gut Phenotype Using Validated Ultra-High-Performance Liquid Chromatography Coupled to Hybrid Orbitrap Mass Spectrometry. *Anal. Chem.* **89**, 12502–12510 (2017).
73. G. Darko, A. Goethals, N. Torto, K. De Clerck, Steady state electrospinning of uniform polyethersulfone nanofibers using a non-heated solvent mixture. *Appl. Nanosci.* **6**, 837–845 (2016).
74. M. Roelants, R. Hauspie, K. Hoppenbrouwers, References for growth and pubertal development from birth to 21 years in Flanders, Belgium. *Ann. Hum. Biol.* **36**, 680–694 (2009).
75. T. J. Cole, Extended international (IOTF) body mass index cut-offs for thinness, overweight and obesity. *Pediatr. Obes.* **7**, 284–294 (2012).
76. L. W. Sumner, A. Amberg, D. Barrett, M. H. Beale, R. Beger, C. A. Daykin, T. W. M. Fan, O. Fiehn, R. Goodacre, J. L. Griffin, T. Hankemeier, N. Hardy, J. Harnly, R. Higashi, J. Kopka, A. N. Lane, J. C. Lindon, P. Marriott, A. W. Nicholls, M. D. Reily, J. J. Thaden, M. R. Viant, Proposed minimum reporting standards for chemical analysis: Chemical Analysis Working Group (CAWG) Metabolomics Standards Initiative (MSI). *Metabolomics*. **3**, 211–221 (2007).
77. D. Monleón, J. M. Morales, A. Barrasa, J. A. López, C. Vázquez, B. Celda, Metabolite profiling of fecal water extracts from human colorectal cancer. *NMR Biomed.* **22**, 342–348 (2009).
78. S. Huysman, L. Van Meulebroek, F. Vanryckeghem, H. Van Langenhove, K. Demeestere, L. Vanhaecke, Development and validation of an ultra-high performance liquid chromatographic high resolution Q-Orbitrap mass spectrometric method for the simultaneous determination of steroidal endocrine disrupting compounds in aquatic matrices. *Anal. Chim. Acta*. **984**, 140–150 (2017).
79. I. Savva, A. S. Kalogirou, A. Chatzinicolaou, P. Papaphilippou, A. Pantelidou, E. Vasile, E. Vasile, P. A. Koutentis, T. Krasia-Christoforou, PVP-crosslinked electrospun membranes with embedded Pd and Cu2O nanoparticles as effective heterogeneous catalytic supports. *RSC Adv.* **4**, 44911–44921 (2014).
80. M. Thirukumaran, V. Singh, Y. Arao, Y. Fujito, M. Nishimura, T. Ogura, J. Pawliszyn,

Solid-phase microextraction- probe electrospray ionization devices for screening and quantitating drugs of abuse in small amounts of biofluids. *Talanta*. **231**, 1–8 (2021).

Acknowledgments

We thank Salma Kasim and Olivier Verschatse, who helped during the experimental work using our LA-REIMS platform and executed SEM analyses, respectively. We thank the Laboratory of Virology (Faculty of Veterinary Medicine, Ghent University, Prof. Nauwynck) for providing colonic and rectal mucosa of slaughtered piglets. We thank UZ Antwerpen (Dr. Van De Maele and Dr. Vermeiren), UZ Brussel (Prof. De Scheper and Prof. Gies), UZ Leuven (Prof. Casteels, Dr. Jacobs and Dr. Rochtus), AZ Jan-Palfijn (Dr. Baeck), AZ Alma (Dr. Vanneste), AZ Sint-Lucas (Dr. Deman), AZ Sint-Jan Brugge (Dr. Depoorter) and OLV van Lourdes Waregem (Dr. De Lille), for their active involvement in the recruitment of children with overweight and obesity. The Laboratory of Integrative Metabolomics (LIMET) research group is part of the Ghent University expertise center MSsmall.

Funding

This work was supported by the following grants: FWO 1S57922N (MDS), FWO 1192622N (KW), ERC FWO Runner-up G0G0119N (LV, MDG), BOF GOA 2017/000102 (KW, NM, SDH and LV), BOF 01J07519 (LV, VP), FWO Hercules AUG/17/09 (LV) and IOF MetaSAMP F2020/IOF-StarTT/066 (LV, KDC, JG, ES).

Author contributions

Conceptualization: MDS, KDC and LV

Methodology: MDS, VP, JG, ES, BP, VS, KDW and LV

Investigation: MDS, KW and ADL

Visualization: MDS, VPa, MDG and LV

Supervision: IG, NM, SDH, KDC and LV

Writing-original draft: MDS and LV

Writing-review & editing: MDS, MDG and LV

Funding: LV, KDC, SDH, NM, MDS and KW

Competing interests

A patent application has been submitted by Ghent University on 31 March 2020, authored by LV, KDC, MDS, JG and VS, and has entered the national phase (WO2021/191467).

Data and materials availability

All data needed to evaluate the conclusions in the paper are present in the paper and/or the Supplementary Materials.

The Supplementary Materials file includes:

Supplementary Notes S1 to S5
Figs. S1 to S19
Tables S1 to S12

Other Supplementary Material for this manuscript includes the following:

Data S1 to S8

Figures and figure captions

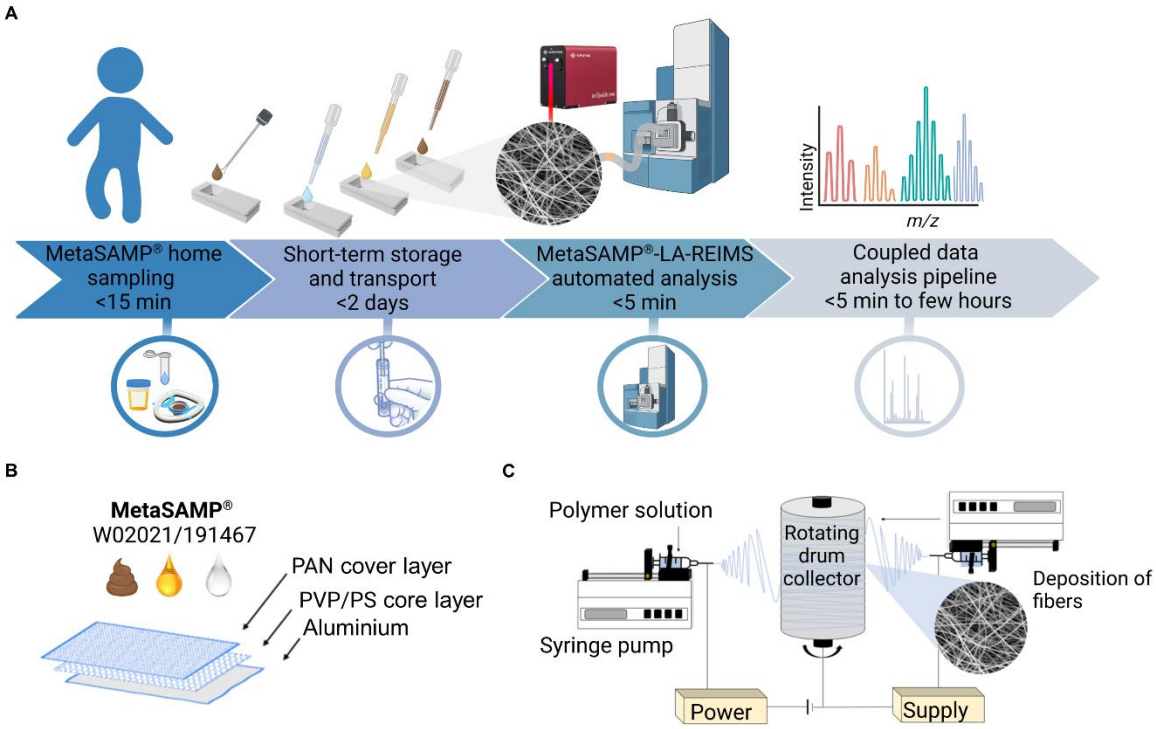

Figure 1. MetaSAMP®-LA-REIMS enables direct rectal, salivary and urinary metabotyping.

(A) A straightforward workflow for MetaSAMP® sampling hyphenated with LA-REIMS analysis. The analytes captured by MetaSAMP® (configured as a sampling kit whether in combination with a medical swab) are desorbed, and the resulting analyte-rich aerosol is directly transferred through a vent line to the inlet capillary, where subsequent quadrupole time-of-flight analysis takes place. Data are visualized in real-time through MassLynx™ software or an in-house data analysis pipeline across the mass range installed, *i.e.*, 50 to 1200 *m/z* range, after which metabolomic alterations can be quickly revealed by multivariate data analysis, leading to first-line segregation and risk classification

based on distinctive fingerprints for decision making in healthcare. (**B)** The 3-layered MetaSAMP® consists of a PAN cover layer, a PVP/PS core membrane, and an aluminium support layer as adhering electrically conductive collector. (**C)** The electrospinning setup consists of a single-nozzle system that is duplicated to enable bidirectional electrospinning of the loaded polymer blends onto a continuously rotating drum.

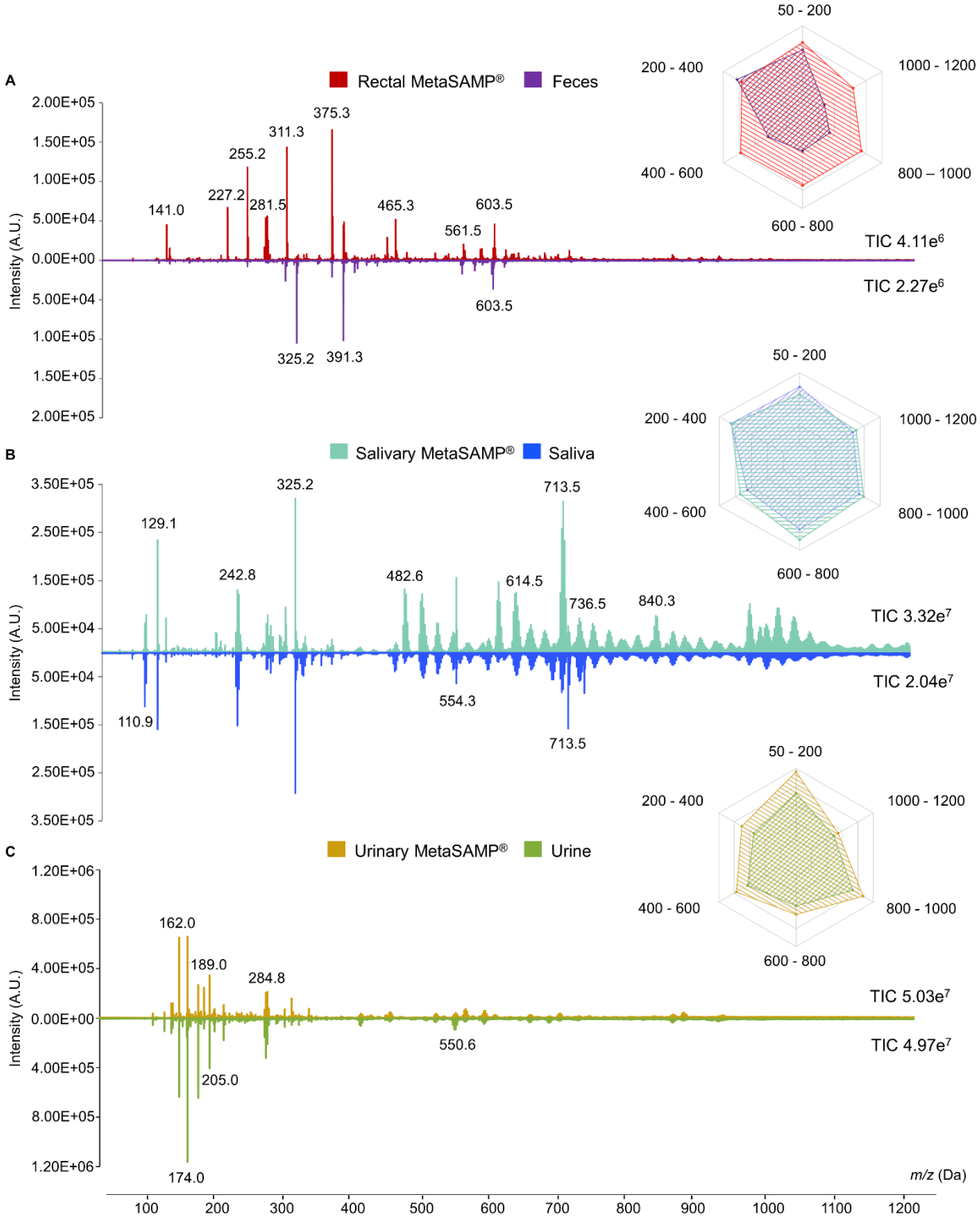

Figure 2. The use of MetaSAMP®s increases the richness and intensity of fecal, salivary and urinary metabolic fingerprints compared to those obtained with crude biofluid LA-REIMS-based metabotyping.

Head-to-tail comparison of LA-REIMS spectra obtained from impregnated **(A)** rectal, **(B)** salivary and **(C)** urinary MetaSAMP®s and feces, saliva and urine, respectively, measured in negative polarity mode (*m/z* range of 50–1200 Da depicted). To accurately compare every crude biofluid and its respective MetaSAMP®, binning of the inspected *m/z* range (0.1 Da) was performed. Average feature intensities (arbitrary units (A.U.)) are shown for the full spectra and the highest intensity peaks were displayed with their specific *m/z* value. TIC values accompany each mass spectrum, representing the overall signal intensities. The selected mirrored mass spectra are representative of the biofluid metabolomes of children and adolescents covering all IOTF scores (MetaBEAse cohort for the rectal and urinary and OPERA cohort (*42*) for the salivary MetaSAMP®s, pooled QC samples, *N*=3). Next to the mirrored mass spectra, radar charts visualize the averaged feature intensities of the crude biofluids (pooled QC samples originating from control children, *N* =3) and their corresponding optimized biofluid-specific MetaSAMP®. The metabolome coverage was subdivided into clinically relevant mass ranges with regard to the metabolic disturbances underlying overweight and obesity (*2*). The colored area represents the metabolome coverage, clearly showing an overlap for every crude biofluid and its specific MetaSAMP®, yet indicating the richness of the latter.

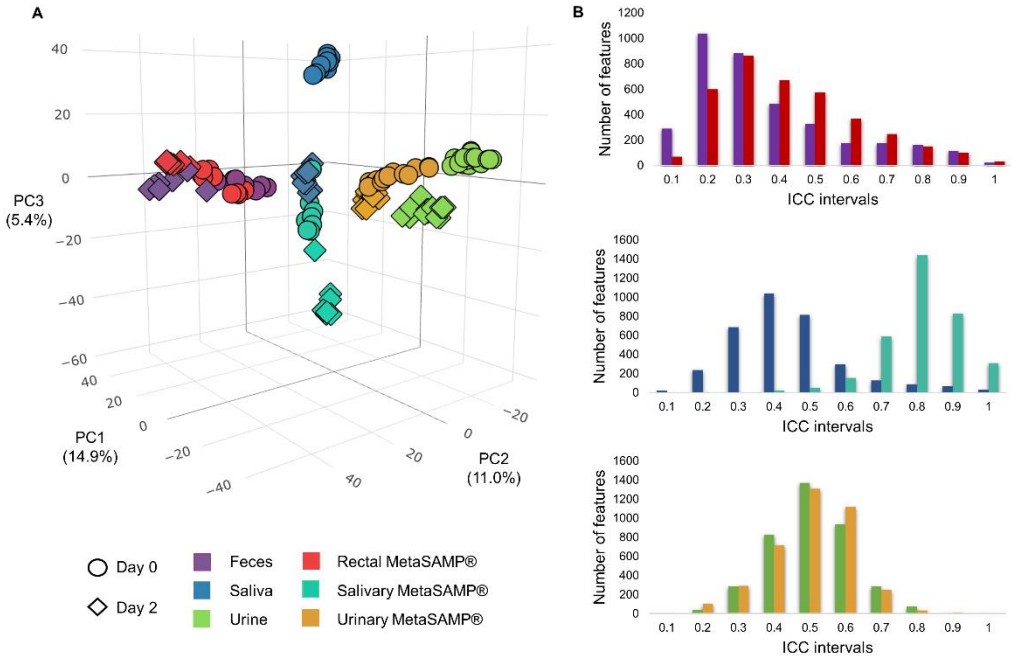

Figure 3. MetaSAMP®s improve short-term (48 h) biofluid-specific metabolome stability as compared to crude biofluid analysis.

(A) 3D-PCA score plots presenting metabolome fluctuations upon storage at 4°C (day 0 *vs.* day 2). The molecular feature count per ICC interval of pooled QC **(B)** fecal, saliva and urine samples, and the corresponding impregnated MetaSAMP®s (*N*=6 per biofluid) analyzed via LA-REIMS are depicted via histograms upon short-term storage at 4°C.

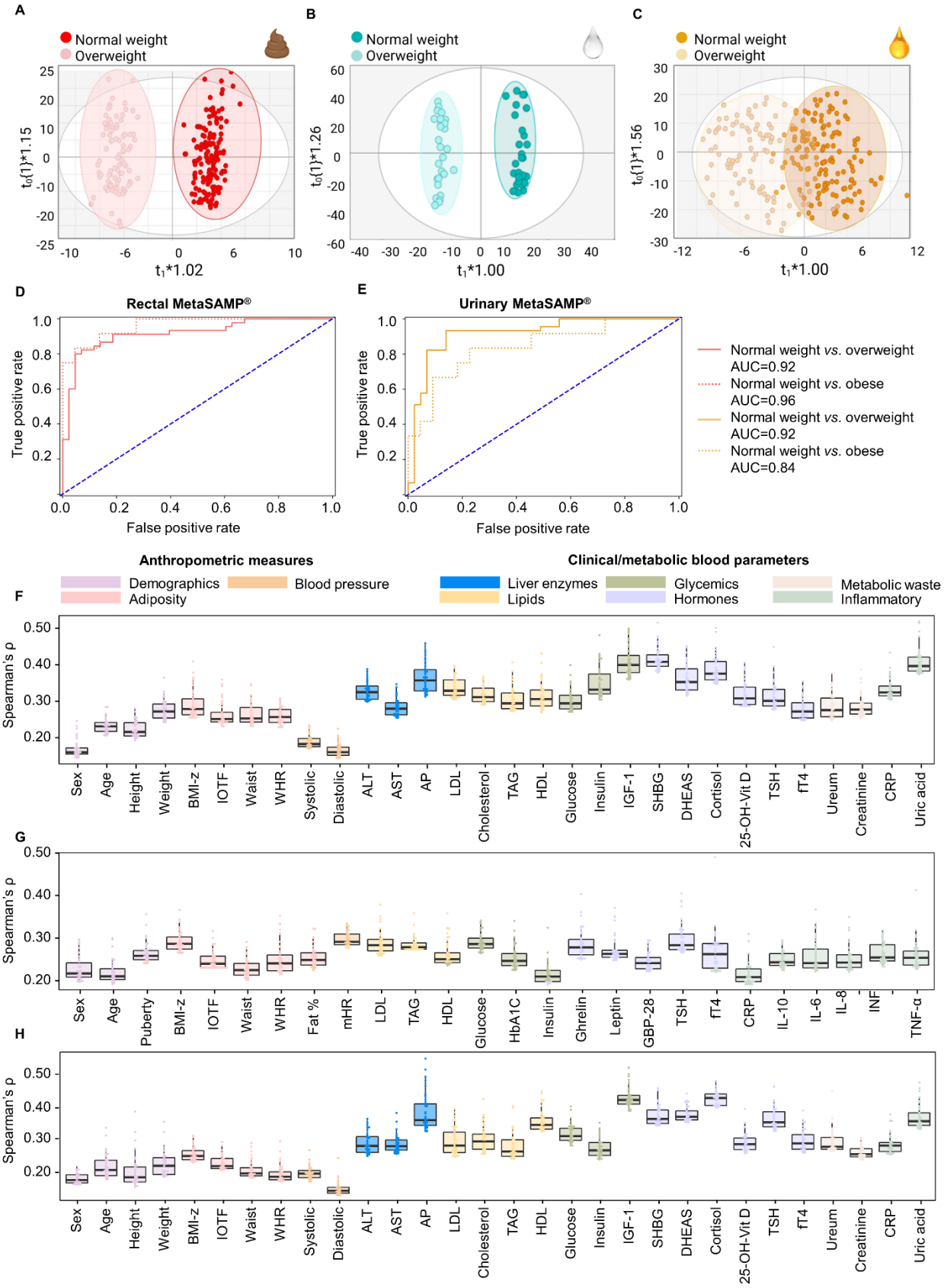

Figure 4. Biofluid-specific MetaSAMP®-LA-REIMS molecular features reflect anthropometric measures and clinical and metabolic blood markers.

(A-C) OPLS-DA score plots as obtained upon LA-REIMS fingerprinting of biofluid-specific MetaSAMP®s with clustering according to weight classification in the patient cohorts, *i.e.*, **(A)** feces (R^2(cum)=0.96, Q^2(cum)=0.63, CV-ANOVA p=1.15e^{-13}), **(B)** saliva (R^2(cum)=0.98, Q^2(cum)=0.53, p=4.05e^{-5}) and **(C)** urine (R^2(cum)=0.64, Q^2(cum)=0.58, p=1.68e^{-11}). ROC curves are plotted using logistic regression analysis to visualize the predictive performance of LA-REIMS analysis in negative polarity mode with **(D)** rectal MetaSAMP® and **(E)** urinary MetaSAMP® based on IOTF classification (N=127 with IOTF=0, N=54 with IOTF=1 and N=34 IOTF≥1). Beeswarm boxplots showing the strongest observed links (anthropometrical measurements and clinical/metabolic blood metadata, *horizontal*) according to Spearman's correlation (*vertical*), with molecular features measured using the **(F)** rectal, **(G)** salivary and **(H)** urinary MetaSAMP®s. Only the 50 strongest (highest modulus Spearman's ρ-value) and significant (p<0.05) correlations of molecular features with anthropometric measures and/or clinical/metabolic blood parameters were included. The interior middle line in the beeswarm boxplots represents the median, lower and upper bounds of the box represent the 25th and 75th percentile values, respectively. Whiskers are drawn from the corresponding box boundary to the most extreme data point located within the box bound±1.5×interquartile range. Beeswarm dots represent Spearman's correlations of individual molecular features with the anthropometric measure or clinical/metabolic blood parameter under investigation.

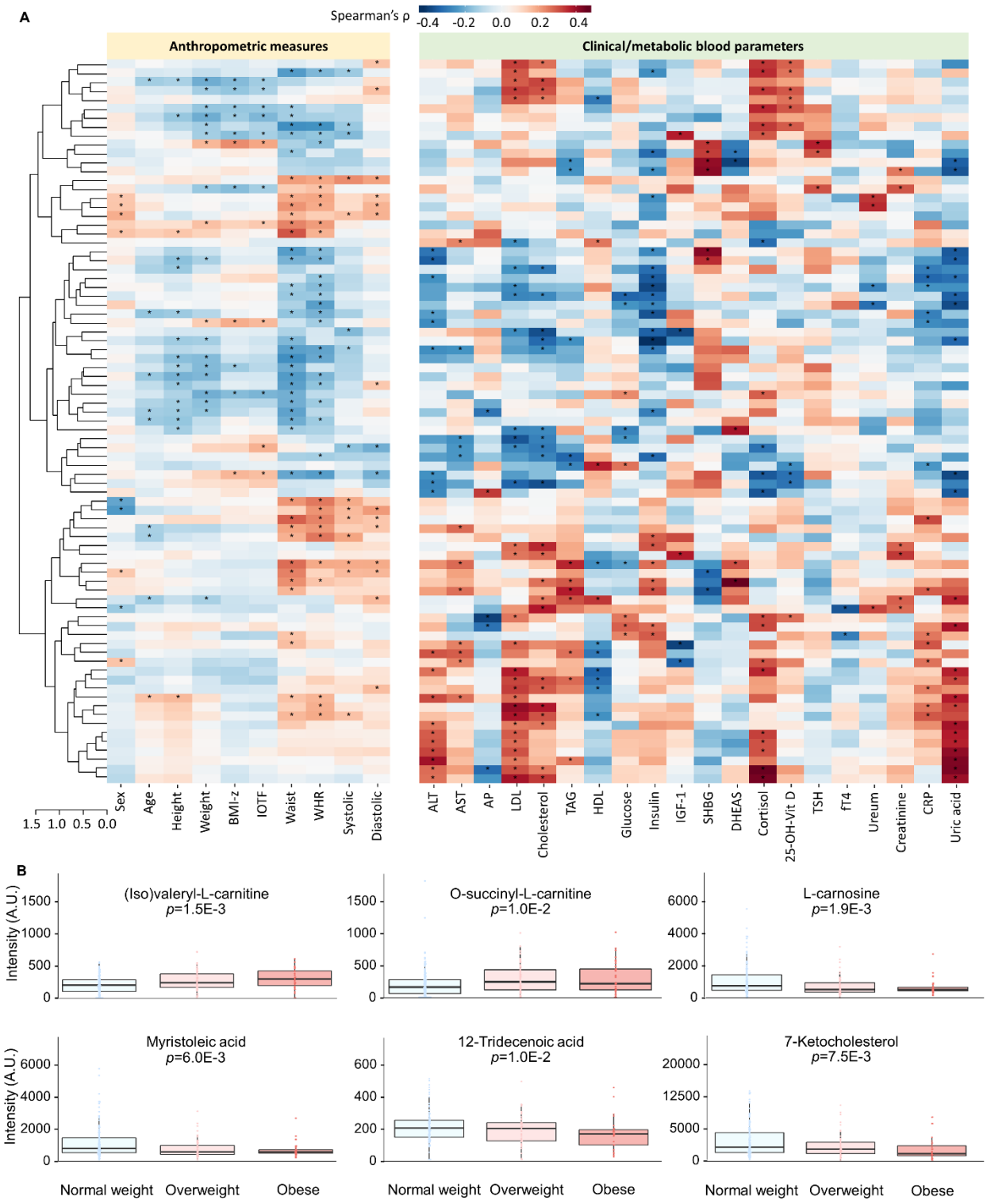

Figure 5. Metabolites detected using rectal MetaSAMP®-LA-REIMS enable individual stratification based on anthropometric and clinical blood markers.

(A) Heatmaps showing relative levels of LA-REIMS (negative ion mode)-derived molecular features that showed significant (Wilcoxon rank-sum tests with continuity correction, $p<0.05$ marked with an asterisk) Spearman correlations with anthropometric measures and/or clinical/metabolic blood parameters from the MetaBEAse cohort.

The molecular features (N=81 unique correlation structures) with the highest correlations (moduli) and at least 4 significant associations (in-between comparisons adjusted $p \leq 0.01$, using FDR correction). **(B)** Beeswarm boxplots of significant ($p<0.05$, Kruskal-Wallis test with Dunn's post-hoc test) discriminatory features between normal weight (IOTF<1), overweight (IOTF=1) and obese (IOTF>1) children. The interior horizontal line represents the median value, lower and upper bounds of the box represent the 25th and 75th percentile values, respectively, and whiskers are drawn from the corresponding box boundary to the most extreme data point located within the box bound± 1.5 × interquartile range. The y-axis of the graphs shows the observed intensity for every adduct that was detected in replicated burns, while the x-axis shows the groups compared. For the multiple comparisons, individual metabolic feature intensities are shown for the different weight groups. Statistical analysis was performed using Kruskal–Wallis with Dunn's post-hoc test for multiple comparisons.

Tables and captions

Table 1. Demographic and anthropometric cohort findings. Data from the MetaBEAse and OPERA (*42*) cohorts comprising overweight and normal weight children and adolescents.

	MetaBEAse		OPERA	
MetaSAMP®	# REIMS analyses			
Rectal	534		NA	
Salivary	NA		372	
Urinary	532		NA	
Demographics	Mean±SD (or expressed in %)			
	# of subjects		# of subjects	
Mean age (years)±SD	234	9.0±2	101	14.0±2
Sex	234	45% female	101	55% female
Puberty				
Tanner stage ≤1	234	100%	7	7%
Tanner stage >1			91	93%
Anthropometrics				
BMI-z scores	234		101	
Range		-3-3		-2-4
≤ -2.0 (underweight)		5 (2.1%)		1 (1.0%)
Between -2.0 and ≤ 1.0 (normal weight)		136 (58.1%)		69 (68.3%)
Between 1.0 and < 2.0 (overweight)		36 (15.4%)		19 (18.8%)
≥ 2.0 (obese)		57 (24.4%)		12 (11.9%)
IOTF	234		101	
Range		-3-3		-1-2
≤-1 (underweight)		19 (8.1%)		4 (4.0%)
0 (normal weight)		127 (54.3%)		66 (65.3%)
1 (overweight)		55 (23.5%)		20 (19.8%)
≥2 (obese)		33 (14.1%)		11 (10.9%)
Waist (cm)	215	67.0±12.6	101	74.6±10.3
WHR	214	0.49±0.07	101	0.45±0.07
Fat (%)	NA		98	23.8±8.7
Systolic BP (mmHg)	215	105.0±14.3	NA	
Diastolic BP (mmHg)	215	67.0±9.6	NA	
Heart rate (bpm)	27	79.4±12.2	86	77.3±10.5

Clinical laboratory tests				
LDL cholesterol (mg dL^{-1})	55	97.0±18.9	75	87.6±21.0
Triglycerides (mg dL^{-1})	64	77.7±35.5	75	81.9±41.8
HDL cholesterol (mg dL^{-1})	63	50.3±10.1	75	59.7±13.7
Fasting plasma glucose (mg dL^{-1})	84	87.6±6.7	75	88.1±6.7
Cholesterol (mg dL^{-1})	64	154.9±16.8	75	159.2±28.1
HbA1c (%)	18	5.3±0.2	76	5.3±0.3
Fasting plasma insulin (pmol L^{-1})	58	80.7±35.7	75	13.3±9.7
TSH (mU L^{-1})	51	2.3±0.8	75	2.4±1.1
fT4 (pmol L^{-1})	43	14.9±2.4	75	15.4±2.2
(hs-)CRP (mg L^{-1})	55	2.1±1.6	76	1.1±1.5
IL-10 (pg mL^{-1})	NA		78	0.4±0.7
IL-6 (pg mL^{-1})	NA		78	0.5±0.5
IL-8 (pg mL^{-1})	NA		78	10.6±5.2
IFN (pg mL^{-1})	NA		78	13.8±43.4
TNF (pg mL^{-1})	NA		78	1.8±0.6
Polymorphonuclear cells (%)	52	49.0±9.2		
Lymphocytes (%)	62	36.3±9.0		
ALT (U L^{-1})	69	19.2±5.6		
AST (U L^{-1})	72	26.4±5.2		
AF (U L^{-1})	29	272.0±60.6		
Ureum (mg dL^{-1})	65	28.1±6.2		
Creatinine (mg dL^{-1})	56	0.5±0.1		
Cortisol (ng mL^{-1})	47	79.0±67.0		
25-hydroxyvitamin D (ng mL^{-1})	47	33.5±19.9		
Uric acid (mg dL^{-1})	36	4.6±0.9		
IGF-1 (µg L^{-1})	31	188.5±55.8		
SHBG (nmol L^{-1})	42	49.1±20.1		
DHEAS (µg dL^{-1})	33	93.9±61.0		

Abbreviations: LDL, low-density lipoprotein; HDL, high-density lipoprotein; HbA1c, hemoglobin A1c; TSH, thyroid-stimulating hormone; fT4, free thyroxine; (hs)-CRP, (highly sensitive) C-reactive protein; IL, interleukin; INF, interferon; TNF, tumor necrosis factor; ALT, alanine transaminase; AST, aspartate transaminase; AF, alkaline phosphatase; IGF-1, insulin-like growth factor 1; SHBG, sex hormone-binding globulin; DHEAS, dehydroepiandrosterone sulfate.